Space: Science & Technology
A SCIENCE PARTNER JOURNAL

REVIEW ARTICLE

Multiscale Modeling Techniques in the Study of 2-Dimensional Materials under Ionizing Radiation

Hongyu Tang[1,2*], Zihao Cai[1], Mengyuan Tang[1], Ninghai Yu[1], Weiqi Shi[1], Lindong Ma[2,3], Jiajie Fan[1*], Rongjun Zhang[1,4], and Guoqi Zhang[5]

[1]College of Intelligent Robotics and Advanced Manufacturing, Fudan University, Shanghai 200433, China. [2]State Key Laboratory of Luminescence and Applications, Changchun Institute of Optics, Fine Mechanics and Physics, Chinese Academy of Sciences, Changchun, Jilin 130033, China. [3]Shanghai Institute of Aerospace Technical Foundation, Shanghai 201109, China. [4]Department of Optical Science and Engineering, Key Laboratory of Micro and Nano Photonic Structures (MOE), Shanghai Engineering Research Center of Ultra-Precision Optical Manufacturing, Fudan University, Shanghai 200433, China. [5]EEMCS Faculty, Delft University of Technology, Delft 2628CD, the Netherlands.

*Address correspondence to: hongyu_tang@fudan.edu.cn (H.T.); jiajie_fan@fudan.edu.cn (J.F.)

Citation: Tang H, Cai Z, Tang M, Yu N, Shi W, Ma L, Fan J, Zhang R, Zhang G. Multiscale Modeling Techniques in the Study of 2-Dimensional Materials under Ionizing Radiation. *Space Sci. Technol.* 2026;6:Article 0403. https://doi.org/10.34133/space.0403

Submitted 24 March 2025
Revised 13 June 2025
Accepted 24 June 2025
Published 22 January 2026

Two-dimensional materials (2DMs)-based devices exhibit aerospace potential due to their superior properties. However, the operational reliability of 2DMs-based devices in space environments is significantly influenced by charged-particle radiation, necessitating rigorous ground-based radiation tolerance assessments. Current research on radiation effects in 2DMs is primarily experimental, yet such methodologies are inherently time-consuming, resource-intensive, and limited in throughput. To address these challenges, computational modeling and simulation techniques are increasingly being integrated with experimental characterization to accelerate materials design and unravel underlying physical mechanisms. This review systematically evaluates the state-of-the-art multiscale computational frameworks for 2DMs research, focusing on recent advancements, technical challenges, and emerging opportunities. A novel integrative approach is proposed, combining density functional theory, molecular dynamics, Monte Carlo, finite element analysis, and machine learning techniques. Particular emphasis is placed on addressing challenges in multiscale modeling, including accurate representation of complex phenomena across spatial and temporal scales under extreme environmental conditions. Conversely, opportunities for enhancing predictive capabilities are highlighted, with implications for expediting materials discovery in electronics, photonics, energy storage, catalysis, and nanomechanical systems. This comprehensive survey provides a strategic roadmap for future research directions in multiscale computational modeling of 2DMs, emphasizing interdisciplinary methodologies that bridge atomistic simulations with macroscale engineering applications. The insights presented herein aim to advance the development of radiation-hardened 2DMs-based devices for next-generation aerospace systems.

Introduction

Devices fabricated from 2-dimensional materials (2DMs) hold great promise in the aerospace field due to their unique mechanical, thermal, electrical, optical, physical, and chemical properties [1]. They have great potential applications in spacecraft, including coating materials, sensors, optoelectronic, and wearable devices. Ionizing radiations induce marked changes to 2DMs, including defect formation, atomic-level doping, interlayer spacing adjustment, and morphological transformation [2]. These changes present opportunities for regulating various properties of 2DMs. The underlying mechanism stems from the complex interaction between incident ions and the target material, which is influenced by multiple factors, including radiation methods (e.g., ion implantation [3], highly charged ions [HCIs] radiation [4], and swift heavy-ion [SHI] radiation [5]), ion types (He, N, B, Si, Ar, etc.), radiation parameters (energy, dose, incident angle, etc.), 2DMs types (graphene, transition-metal dichalcogenides [TMDs], heterostructures, etc.), and the substrates.

To investigate the radiation effects on 2DMs-based devices, lots of experimental techniques are employed to study the electrical and optical properties of 2DMs under different radiation doses, e.g., Raman spectroscopy, photoluminescence (PL) spectroscopy, transmission electron microscopy (TEM), friction force microscopy, and Kelvin probe force microscopy (KPFM) [6]. Nevertheless, these methods are time-consuming, costly, and inefficient. As a result, an increasing number of computational modeling and simulation techniques are being utilized to complement experimental synthesis, characterization, and testing for accelerating the research and design of 2DMs and analyzing the mechanisms [7,8], or calculate material properties that are difficult, if not impossible, to determine experimentally [9,10]. For

instance, by combining density functional theory (DFT) and machine learning force fields (MLFFs), the Raman spectrum of MoS_2 with defect distributions can be simulated, further validating that sulfur vacancies are the main type of defects [11]. These computational models and simulations enable in-depth exploration of the structure, properties, behavior, and functions of materials at various time and spatial scales, and can identify specific properties or phenomena in complex experimental setups.

This review systematically evaluates the state-of-the-art advancements in multiscale modeling techniques for understanding the radiation response of 2DMs under diverse ionizing radiation scenarios. First, we characterize the space radiation environments and their induced degradation mechanisms, including displacement damage and ionization effects. Subsequently, we analyze the performance alterations of 2DMs and their device architectures under proton, electron, and heavy-ion irradiations. Particular emphasis is placed on evaluating computational modeling methodologies that enable accelerated exploration of structure–property relationships in radiation-affected 2DMs. We present a hierarchical modeling framework spanning atomistic to mesoscopic scales, integrating DFT, ab initio molecular dynamics (AIMD), classical molecular dynamics (MD), Monte Carlo (MC), finite element analysis (FEA), and machine learning (ML) techniques. Fig. 1 illustrates the proposed integrative multiscale approach, which couples atomic-scale defect simulations with mesoscale device performance predictions. We aim to discuss the possibility of comprehensively designing new 2DMs under computational guidance, reduce expensive and time-consuming trial-and-error experiments, and prospect the computational design tools for 2DMs-based devices suitable for aerospace applications.

A Short Background of 2DMs in Space Radiations

The space radiation environment

The space radiation environment can be categorized into 3 primary types [12]. (a) Van Allen radiation belts (Earth's radiation belts): These toroidal regions comprise high-energy electrons, protons, and trace heavy ions trapped by Earth's geomagnetic field. The inner belt is dominated by energetic protons (>10 MeV), while the outer belt is populated by relativistic electrons (>0.1 MeV); (b) Solar cosmic rays (SCRs): Energetic particle streams emanating from solar active regions, predominantly during solar flares and coronal mass ejections (CMEs). Composed primarily of protons (~90%) with energies ranging from tens of keV to several GeV, SCR events are often termed solar proton events (SPEs) due to their proton-rich composition; (c) Galactic cosmic rays (GCRs): Highly energetic charged particles originating from beyond the solar system, consisting predominantly of fully ionized atomic nuclei. GCRs exhibit a composition of ~87% hydrogen nuclei (protons), ~12% helium nuclei (alpha particles), and ~1% heavier nuclei (e.g., C, N, O, and Fe). Despite their ultrahigh kinetic energies (up to ~1,020 eV), GCR fluxes follow a steep power-law decline with increasing energy, rendering high-energy particles extremely rare.

Radiation effects on electronic components can be systematically classified into 2 primary categories [13]. (a) Ionization damage (total ionizing dose [TID] effect): This mechanism involves the accumulation of charge carriers in dielectric materials, manifested as interface trap charges and oxide trap charges induced by particle radiation. These charges alter the electrical characteristics of semiconductor devices (e.g., threshold voltage shifts in metal-oxide-semiconductor field-effect transistors) by disrupting charge balance at material interfaces; (b) Displacement damage: Characterized by the disruption of crystalline lattice structures in semiconductors, this mechanism introduces lattice defects (e.g., vacancies, interstitials, and Frenkel pairs) through nuclear collisions with incident particles. Such defects degrade carrier lifetime and mobility, leading to progressive performance degradation in electronic components. In general, the TID effect is the dominant factor that affects performance of electronic components. In optoelectronic devices, e.g., solar cells, displacement damage has a more pronounced impact. Consequently, solar cell arrays intended for space applications have to undergo ground-based 1-MeV electron radiation testing to evaluate their susceptibility to space radiation. A summary of key space environmental effects on electronic systems is presented in Table 1.

Types of ionizing radiation

Ionizing radiation is defined as the propagation of energy through atomic/subatomic particles or electromagnetic waves with sufficient energy to ionize atoms by ejecting bound electrons, resulting in charged atomic species. This category encompasses high-energy electromagnetic radiation (e.g., γ-rays and x-rays) and particulate radiation including electrons, protons, neutrons, and alpha particles.

Gamma (γ) radiation

γ-rays possess energy levels exceeding approximately 100 keV. The Compton scattering can generate high-energy free electrons and positive ions in solid materials. These free electrons interact with atoms, resulting in ionization, atomic displacement, and the formation of vacancies and interstitials. γ-rays can modulate the Dirac voltage of graphene field-effect transistors (GFETs), enabling their use in radiation detection. At low doses, γ radiation can increase carrier density, while medium doses induce maximum structural disorder. Furthermore, γ-rays are utilized in generating reduced graphene oxide (rGO).

X-ray ionization radiation

X-rays have energy levels ranging from approximately 100 eV to 100 keV. They can induce ionization defects, e.g., vacancies in semiconductors, and facilitate the reduction of graphene oxide (GO). Compared to γ-rays, a higher dose of x-rays is required to achieve an equivalent reduction effect.

Electron ionization radiation

Electrons interact with materials via elastic and inelastic scattering, leading to displacement, sputtering, heating, charging, radiolysis, and radiation-induced contamination. In 2DMs, electrons can cause metal sputtering, atomic displacement, and ionization decomposition, as well as charging of insulators and semiconductors. Electron beam radiation within a TEM can produce defect structures in graphene.

Neutron ionization radiation

Neutron ionization radiation is primarily the result of nuclear reactions. Fast neutrons damage materials through cascade scattering effects, where initial collisions cause displacement and ionization, restricting damage in 2DMs to the nanoscale.

Ion ionization radiation

Ion ionization radiation can induce degradation defects and simulate damage similar to that caused by nuclear reactors or cosmic rays. Ion beam radiation replicates ionization radiation

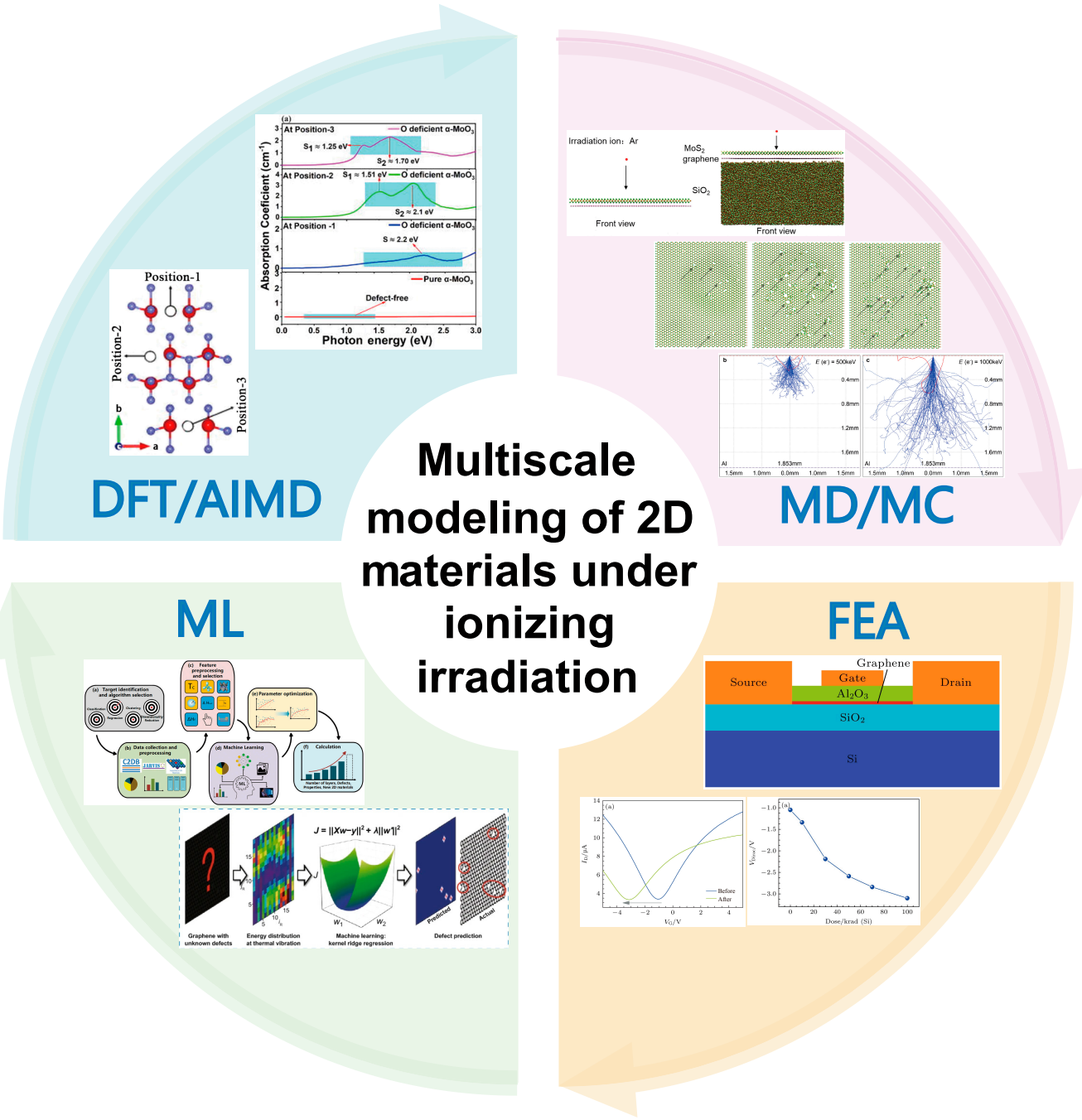

Fig. 1. Overview of multiscale modeling techniques for 2DMs under ionizing radiation. The density functional theory (DFT)/ab initio molecular dynamics (AIMD) images are reprinted with permission from Ref. [31]. Copyright 2021, Springer Nature Publishing. The molecular dynamics (MD)/Monte Carlo (MC) images are reprinted with permission from Ref. [14, 59]. Copyright 2019, 2021, Springer Nature Publishing. The finite element analysis (FEA) images are reprinted with permission from Ref. [105]. Copyright 2024, Science Press. The machine learning (ML) images are reprinted with permission from Ref. [114, 118]. Copyright 2020, Springer Nature Publishing and Copyright 2024, Wiley Publishing.

effects encountered in reactors, enabling accelerated studies of radiation damage by rapidly degrading samples.

The effects of ionizing radiation on 2DMs

High-energy ionizing irradiation induces defects that can compromise both the structural stability and electrical characteristics of materials. Characterizing the effects of these radiation-induced imperfections is critical for advancing 2DMs-based technologies designed for extreme radiation conditions, such as space applications or nuclear reactor systems. Therefore, the majority of experimental investigations concentrate on evaluating TID damage in 2DMs and related devices. Current research efforts utilize various radiation sources in TID testing, including x-rays, γ-rays, electrons, protons, and heavy ions, to analyze the response of 2DMs-based technologies to ionizing radiation [14]. The effects of radiation environments on these devices are primarily manifested through incident ionizing radiation in the forms of photons, neutrons, or charged particles. Such radiation creates structural defects within the material matrix, leading to performance degradation in functional devices. Additionally,

Table 1. The space environmental effects [119]

Mechanism	Effect	Source
Surface charging	Biasing of instrument readings Power drains Physical damage	Dense, cold plasma Hot plasma
Deep dielectric charging	Biasing of instrument readings Electrical discharges causing physical damage	High-energy electrons
Structure impacts	Structural damage Decompression	Micrometeoroids Orbital debris
Drag	Torques Orbital decay	Neutral thermosphere
Total ionizing dose (TID)	Degradation of microelectronics	Trapped protons and electrons Solar protons
Displacement damage dose (DDD)	Degradation of optical components and some electronics Degradation of solar cells	Trapped protons and electrons Solar protons Neutrons
Single-event effects (SEE)	Data corruption Noise on images System shutdowns Electronic component damage	GCR heavy ions Solar protons and heavy ions Trapped protons Neutrons
Surface erosion	Degradation of thermal, electrical, optical properties Degradation of structural integrity	Particle radiation Ultraviolet Atomic oxygen Micrometeoroids contamination

photons with lower energy levels (e.g., terahertz, infrared, visible, and ultraviolet spectra) can also influence device characteristics. Notably, the ionization phenomena caused by high-energy photons (e.g. x-rays and γ-rays) merit particular attention due to their unique interaction mechanisms with 2DMs.

It is well known that defects in semiconductor lattices alter device performance, typically degrading it. The impact of ionizing radiation effects is summarized in Table 2. Due to the destructive nature of cosmic rays, their radiation effects need to be carefully considered in space applications. 2DMs exhibit a relatively low probability of interaction between ions and the 2-dimensional (2D) atomic layers [15,16]. Thus, high-energy ion damage primarily occurs in the substrate, leading to the formation of various defects near the interface between the substrate and the 2DMs, e.g., generation/recombination centers, traps, compensators, and tunneling states. Each of these defects considerably influences device performance. In 2DMs, generation centers play a dominant role, while in heavily doped materials, recombination centers are more critical. Defects located near the middle of the bandgap have the most important impact on material properties.

These radiation-induced defects arise from 2 primary mechanisms: ionization-induced charge trapping and displacement damage via knock-on atomic collisions. Ionization effects result in the generation and accumulation of mobile holes and electron traps within gate dielectric layers (e.g., SiO_2), followed by charge neutralization at the semiconductor–oxide interface. This process leads to pronounced threshold voltage shifts, as characterized in

Table 2. The impact of ionizing radiation effects on 2DMs [15,16]

Defects	Particles	Influences
Generation bit Composite bit	Heavily charged particles	Scattering, carrier concentration modulation
Trap state	Heavily charged particles	Scattering, reduced carrier lifetime, charge accumulation
Tunneling	Heavily charged particles, ion beams	Defects, leakage current
Doping	Heavily charged particles	Scattering, charge accumulation
Vacancies	Electrons, ion beams, x-rays, γ-rays	Deep energy level traps, direct to indirect band gap transition
Superposition states	Heavily charged particles, γ-rays	Scattering, reduced carrier lifetime, charge accumulation

SiO_2-based devices [17]. Electric-field-assisted thermal annealing is commonly employed to mitigate radiation damage in hardened oxides, where the recovery efficiency depends on both the applied bias field and oxide thickness. However, when the trapped charge density exceeds critical thresholds (e.g., >50% of generated holes remain trapped rather than being collected), complete annealing becomes unattainable. Prolonged oxide recovery times are observed with higher trap densities, necessitating that SiO_2 maintains a trapped hole fraction below 10% to preserve radiation hardness. Si-based photodetectors and field-effect transistors (FETs) typically exhibit degradation through 2 distinct failure modes: (a) threshold voltage instability due to charge trapping in gate dielectrics and (b) long-term mobility degradation caused by defect scattering in channel regions. While near-interfacial defects may initially have minimal impact on carrier transport, their cumulative effects eventually lead to catastrophic device failure. Specifically, FETs demonstrate a logarithmic degradation trend under prolonged irradiation, attributed to defect-induced phonon scattering and carrier trapping dynamics. These findings highlight the critical need for multiscale modeling approaches that couple atomic-scale defect formation with mesoscale transport simulations to predict device reliability in radiation environments.

Structural modulations

At present, several technologies are employed to modulate the band structures, charge densities, density of states (DOS), and lattice symmetries for 2DMs, enabling the construction of 2DMs-based devices with specific functions and excellent performances. Ionizing radiation is regarded as one of the important ways to modulate 2DMs' crystal structures, including defect generation, doping effects, interlayer distance reduction, and folding effects [18,19].

Defect generation

Common defects in 2DMs include vacancies, anti-sites, substitutions, and grain boundaries, among others. Although these defects are often considered to have negative impacts, controlling their types and concentrations can achieve beneficial functions. Ionizing radiation can effectively construct the defect engineering of 2DMs. Under electron-beam radiation, lattice vibrations play an important role in atomic displacement. Proton radiation increases the interlayer distance of rGO paper, leading to a decline in thermal stability and electrical performance, while it reduces the interlayer distance of GO paper. He^+ ion radiation makes the defect density of graphene positively correlated with the radiation dose, and an excessively high dose can cause a structural transformation. In TMDs (e.g., MoS_2, $MoSe_2$, etc.), the radiations by electron beams, plasmas, Au ions, γ-rays, proton beams, neutron beams, etc., can also generate defects, considerably changing their PL, electrocatalytic, optical, frictional, and electrostatic properties. Fig. 2A shows the structure, formation, and evolution of rotational defect in WSe_2 [20].

Doping effects

Compared with traditional doping methods that require chemical reagents and are prone to introducing pollutants, doping induced by ionizing radiation has advantages of universality and positionability, and it is an effective doping method in the semiconductor industry. For 2DMs, low-energy radiation can achieve doping and avoid the negative impacts of over-radiation. Ion implantation can introduce dopants and defects in graphene to regulate the bandgap. It has successfully doped impurity atoms (e.g., boron and nitrogen) uniformly into the graphene lattice, changed its electronic structure, and regulated the band structure. However, impurity atoms and lattice defects can cause weak localization of carriers in graphene at low temperatures, resulting

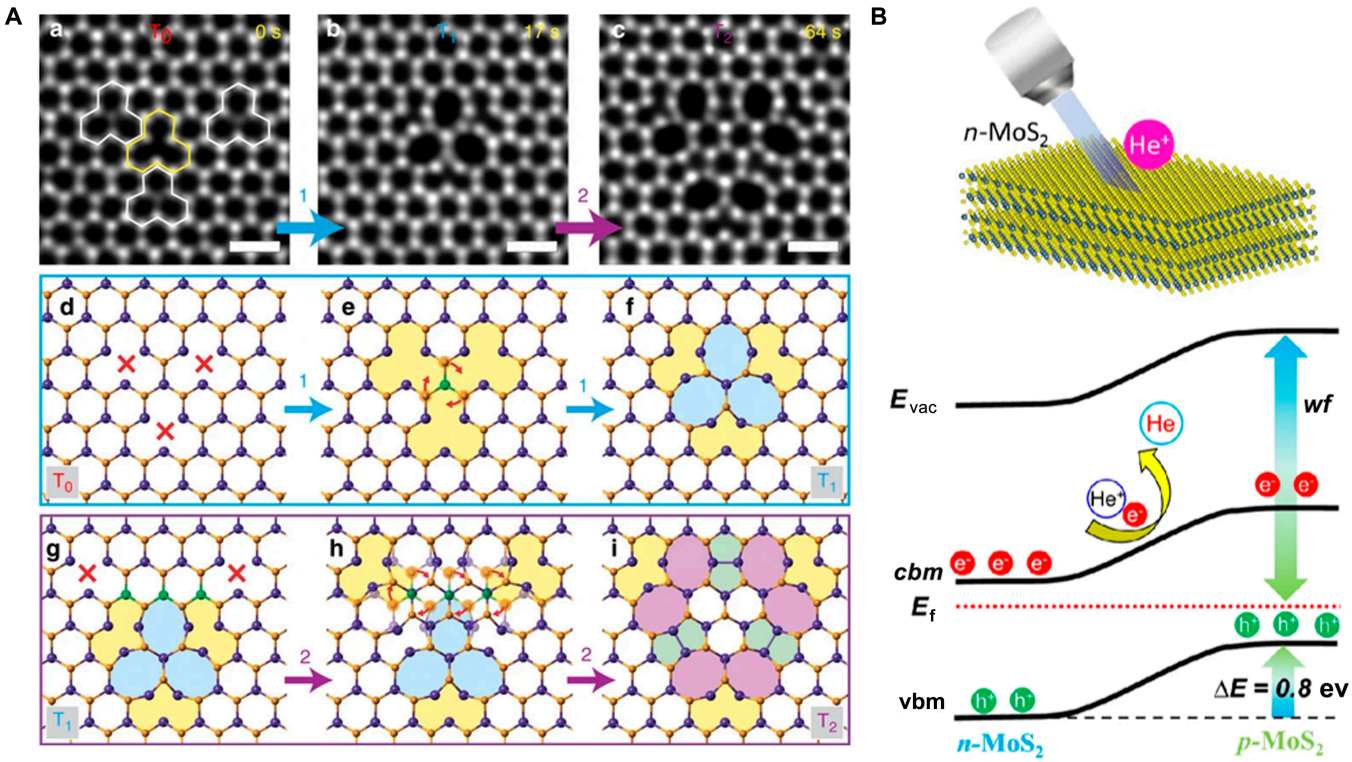

Fig. 2. The ionizing radiation induced (A) defects [20] and (B) doping effects [21].

in a decrease in mobility and electrical conductivity. Additionally, low-energy He^+ ion radiation of MoS_2 can form hole doping, and an H^+ ion beam with keV-level energy can generate n-type doping in the layered WSe_2 structure, improving the electrical and optical properties of the materials [21].

Spatial structure effects

Ion-beam treatment can achieve the compression and folding effects of the lattice structure of 2DMs. Ion radiation can compress the interlayer of few-layer graphene nanosheets, enhancing the interaction with the evanescent field and improving the polarization-dependent light-absorption ability. β-particle, γ-ray, and α-particle radiations of GO can reduce the interlayer distance. By adjusting radiation conditions, e.g., ion energy, dose, and incident angle, the morphology and distribution of the folding structure of 2DMs can be precisely controlled [22]. The synergy of ion-beam radiation and thermal annealing treatment can also form adjustable-sized protrusions and bubbles [23].

Physical property modulations

The introduction of defects and doping into the 2DMs can greatly affect their physical properties, e.g., carrier transport characteristics, band structure, and bandgap, thereby profoundly influencing the material's electrical, optical, and mechanical performance. By precisely controlling the type, concentration, and distribution of defects and doping within the material, it is possible to achieve fine-tuned optimization of 2DMs properties. This modulation offers broad prospects for the application of 2DMs in optoelectronic devices and mechanical systems. However, it is also crucial to manage the scale of defects and doping to avoid adverse effects on material properties.

Electrical properties

Defects and doping induced by ionizing radiation can affect the carrier mobility of 2DMs, thereby influencing the performance of optoelectronic devices. Different ions (e.g., heavy ions, neutrons, protons, and He^+ ions) and irradiation fluences have varying effects on electrical properties. Low-fluence heavy ion irradiation is able to repair the defects to enhance conductivity, while high fluences may introduce excessive defects that disrupt the lattice structure, leading to performance degradation. Light ion irradiation can modulate electrical properties, while neutron irradiation can achieve substitutional doping, altering carrier dynamics. The electrical performance of MoS_2 FETs is differentially affected by proton and He^+ ion irradiation at varying fluences [24] (Fig. 3A).

Optical properties

Ion irradiation induces microstructural evolution in 2DMs, substantially impacting their optical properties. Carbon and oxygen ion beam irradiation can reduce the interlayer spacing of graphene, improving the performance of waveguide lasers. Heavy ion irradiation provides nonradiative recombination channels for excitons in MoS_2, altering its PL spectrum. Argon ion irradiation can directionally modulate the optical properties of WS_2, while oxygen plasma treatment enhances the PL intensity of monolayer MoS_2. γ radiation modifies the Raman spectrum and PL intensity of WS_2, and focused ion beams can tune the optical properties of large-area monolayer WS_2 (Fig. 3B) [25,26].

Magnetic properties

Ion beam irradiation can control the magnetic properties of 2D magnetic materials. Low-energy boron, nitrogen, and carbon ion irradiation can alter the magnetic transport properties of graphene films. Different ions (e.g., niobium, cobalt, and nickel) and irradiation parameters have varying effects on the magnetic properties of MoS_2. γ-ray irradiation can induce room-temperature ferromagnetism in few-layer MoS_2 films (Fig. 3C) [27].

Mechanical properties

Defects introduced by ion irradiation considerably affect the mechanical properties of 2DMs. Argon ion irradiation of monolayer graphene initially increases its 2D elastic modulus with increasing ion concentration, followed by a decrease, while the fracture force first drops sharply and then stabilizes. He^+ ion irradiation of bilayer and 5-layer graphene initially increases the Young's modulus before decreasing it, though the material retains excellent performance. Argon ion irradiation of MoS_2 reduces its fracture stress, strain, and Young's modulus (Fig. 3D) [28,29].

The type and energy of ionizing radiation are critical determinants of 2DMs property modulation, with charged particles (e.g., protons and ions) and neutral particles (e.g., neutrons) interacting through distinct mechanisms. Charged particles exceeding the ionization threshold (~keV) ionize lattice atoms via Coulomb interactions to create primary defects, while subthreshold particles transfer kinetic energy to electrons triggering cascading ionization events. Photons such as γ/x-rays undergo photoelectric absorption or Compton scattering, generating electron–hole pairs and Auger electrons. Radiation effects are energy-dependent: low-energy irradiation (<100 keV) dominates nuclear stopping, causing surface amorphization, ion implantation, and defect clustering through nuclear collisions for controlled doping and nanostructure formation; medium-energy irradiation (100 keV to 1 MeV) transitions to significant electronic stopping via electron excitation near 1 MeV, producing synergistic nuclear-electronic energy deposition for complex defect landscapes and bandgap engineering; fast heavy ion irradiation (>1 MeV/u) dominates electronic stopping, creating highly localized thermal spikes (10^4 to 10^6 K) that induce amorphization tracks or phase transitions, making it effective for ordered nanostructure creation in layered materials. This energy-dependent interaction continuum enables precise control over defect generation, doping profiles, and structural modifications in 2DMs for advanced device applications.

Computational Techniques of 2DMs under Ionizing Radiation

Theoretical frameworks have been developed to characterize ion irradiation-induced material degradation mechanisms. Among these, atomistic computer simulations, which resolve atomic-scale interactions and defect formation dynamics, serve as a cornerstone for understanding radiation damage processes at the fundamental level. These methods, including MD and MC simulations, can accurately model ion–solid interactions, defect clustering, and microstructure evolution. However, their applicability to large-scale systems is constrained by inherent computational intensity, typically limited to submicrometer length scales. Conversely, multiscale modeling approaches address this limitation through hierarchical integration of atomistic simulations with continuum mechanics. By coupling atomic-scale defect generation with mesoscopic transport phenomena, these hybrid frameworks enable predictive modeling of irradiation effects across multiple orders of magnitude. This synergy allows for more realistic representation of damage

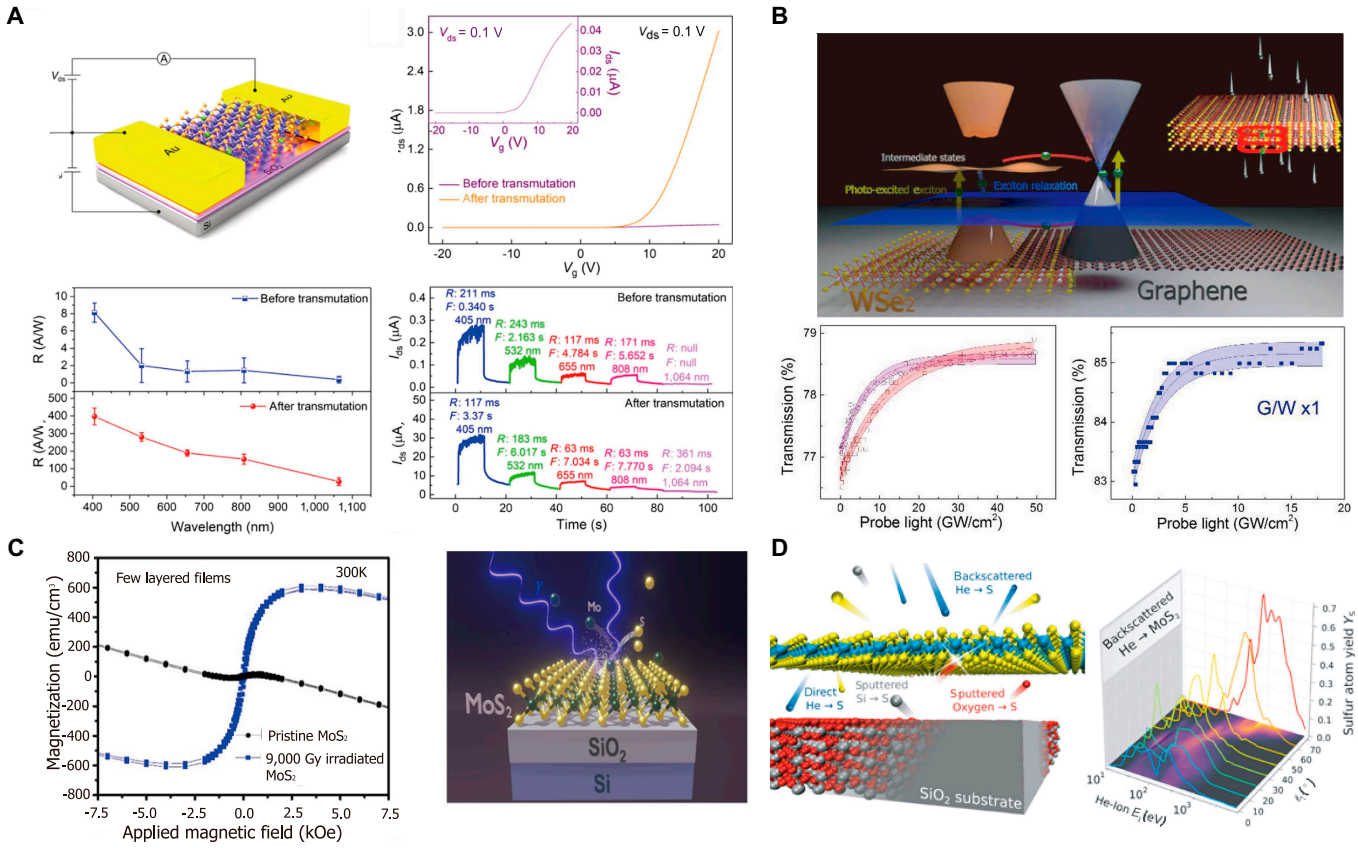

Fig. 3. Ionization radiation controlled (A) electrical [24], (B) optical (adapted with permission from Ref. [25]; Copyright 2017 American Chemical Society), (C) magnetic (adapted with permission from Ref. [27]; Copyright 2018, American Chemical Society), and (D) mechanical properties (reprinted with permission from Ref. [28]; Copyright 2023, American Chemical Society).

accumulation processes while maintaining computational tractability. This section presents different computational techniques of 2DMs under ionizing radiation.

Electronic scale calculations

Ion irradiation induces surface defects in 2DMs due to their relatively low binding energies. Compared to transition metal atoms, chalcogen atoms in 2D crystals are more susceptible to displacement under ion irradiation, generating defective structures. As a first-principles quantum mechanical method, DFT enables accurate prediction of ground-state properties and provides critical insights into defect effects in 2DMs. DFT elucidates how defects influence structural, electronic, and optical characteristics, making it indispensable for interpreting experimental observations of defect phenomena, including magneto-optical measurements. The vacancy formation energy can be calculated as follows [30]:

$$E_{\mathrm{VFE}} = E_{\mathrm{defect}} - E_{\mathrm{perfect}} + \sum n_i \mu_i \quad (1)$$

As shown in Fig. 4, Kumar et al. [31] explored defect engineering in H^+ irradiated layered α-MoO_3 flakes through first-principles calculations and Bader charge analysis to identify the origin of new PL peaks. Using Ehrenreich–Cohen formalism, composite dielectric functions were employed to compute optical absorption coefficients for defective and pristine α-MoO_3. It indicated that oxygen vacancies at distinct α-MoO_3 sites induce new absorption peaks in the ~2.2 to 1.25 eV range. Entani et al. [32] demonstrated a nonchemical method for heteroatom doping in h-BN via high-energy ion irradiation. First-principles calculations on fluorinated sp^3-hybridized BN revealed that F-atom adsorption induces sp^2-to-sp^3 hybridization transitions in host atoms, elongating bonds between sp^3- and sp^2-hybridized atoms on h-BN basal planes and causing buckling in fluorinated regions. Electron spectroscopy for chemical analysis code under the final-state single-electron approximation reproduced experimental near edge x-ray absorption fine structure spectroscopy, including the emergence of peak iii and broadening of peaks β and γ. Peak ii intensity was attributed to substitutional defects, while peak iii—exclusive to fluorinated h-BN on Cu substrates—originated from electron density redistribution due to fluorine's high electronegativity. Peak iv correlated with hybridization between BN pz and Cu d orbitals.

As shown in Fig. 5A, Yao et al. [33] systematically investigated secondary electron (SE) emission from graphene using real-time time-dependent DFT (RT-TDDFT) simulations coupled with proton irradiation experiments (0.2 to 80 keV). Their study revealed a direct correlation between lattice temperature and enhanced SE emission yields. Specifically, the thermal characteristics of the substrate and its thermal coupling efficiency with the 2DM were identified as critical modulators of lattice temperature within the graphene layer. This thermal interplay indirectly influences SE yield and energy distribution by altering local ionization dynamics and charge balance mechanisms, underscoring the nonnegligible role of thermally driven processes in radiation–matter interactions at the nanoscale. Lin et al. [34] proposed polarity conversion and transport modulation in 2D TMDs via controlled

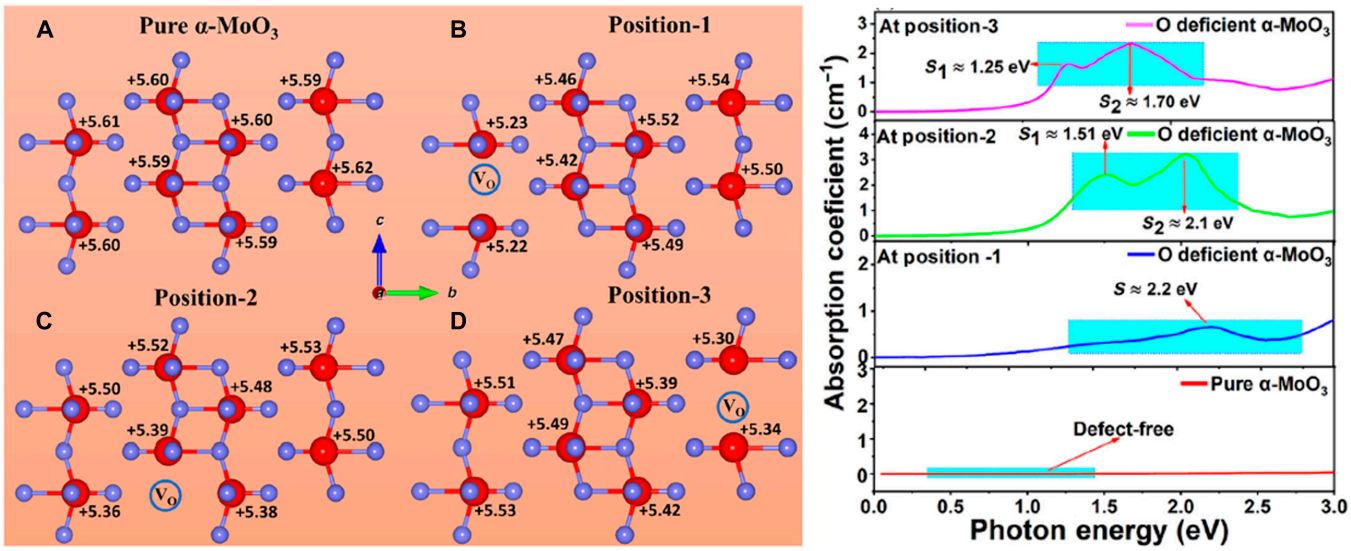

Fig. 4. Charge analysis on Mo atoms in (A) pure α-MoO_3 and α-MoO_3 with oxygen vacancy at different locations in the supercells: (B) position-1, (C) position-2, and (D) position-3. The corresponding absorption coefficients for these configurations are shown in the right panels [31].

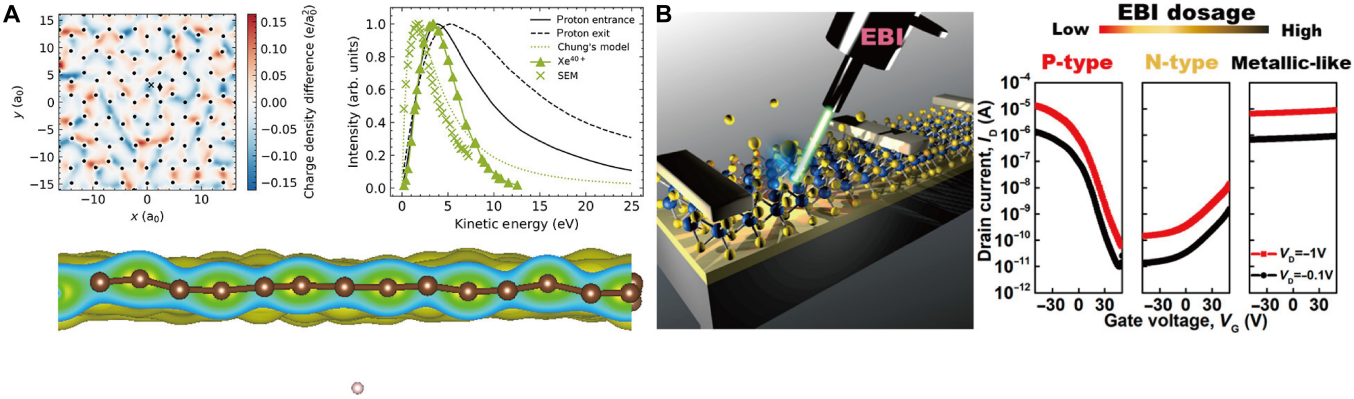

Fig. 5. (A) Comparison of simulated kinetic energy spectra with a measured spectrum for Xe^{40+} ions impacting graphene (reprinted with permission from Ref. [33]; Copyright 2024, American Chemical Society). (B) Evolution of transfer curves in a 2H-$MoTe_2$ back-gate FET under cumulative EBI dose (reprinted with permission from Ref. [34]; Copyright 2019, American Chemical Society).

electron-beam irradiation (EBI) (Fig. 5B). EBI-generated intrinsic chalcogen vacancies in MoS_2 and $MoTe_2$, with DFT simulations showing chalcogen-deficient TMDs, induce defect states near conduction band edges (CBEs). Increasing sulfur/tellurium vacancy concentrations caused CBE downshifts and bandgap narrowing. Defect states near band edges originated from Mo *d*-orbital dangling bonds and weakened Mo 4*d*-chalcogen *p*-orbital hybridization. Native chalcogen vacancies substantially reduced TMD bandgaps, with n-type conduction enhancement in both materials. At critical vacancy concentrations (5×10^{14} cm^{-2} for MoS_2; 4×10^{14} cm^{-2} for $MoTe_2$), bandgap collapse due to defect-state proliferation correlated experimentally with metallic conduction. $MoTe_2$ exhibited sequential p-type to n-type to metal-like conduction transitions under increasing EBI doses.

MD simulations

Energy transfer model from energetic ions to 2DMs

The energy transfer mechanisms during ion irradiation of 2DMs can be categorized into 2 dominant processes: nuclear stopping and electronic stopping. Nuclear stopping originates from elastic collisions between incident ions and target nuclei, whereas electronic stopping results from inelastic interactions between projectiles and the electron system within the 2D lattice [35–37]. As demonstrated in Fig. 6, these processes exhibit energy-dependent dominance, with nuclear stopping prevailing at lower ion energies and electronic stopping becoming predominant at higher energy regimes.

The nuclear stopping component describes elastic scattering phenomena, typically modeled through sequential binary collision approximations. The fundamental scattering parameters can be derived using the center-of-mass formulation:

$$\theta(p) = \pi - 2\int_{r_{\min}}^{\infty} \frac{p\,dr}{r^2\left[1 - \frac{V(r)}{E_{CMS}} - \frac{p^2}{r^2}\right]^{1/2}} \quad (2)$$

where p is the impact parameter, $V(r)$ is the scattering potential, and E_{CMS} corresponds to the center-of-mass energy. The energy transfer during collisions follows:

$$T(p, E_{CMS}) = \frac{4m_1}{m_1 + m_2} E_{CMS} \sin\left(\frac{\theta_{CMS}(p, E_{CMS})}{2}\right)^2 \quad (3)$$

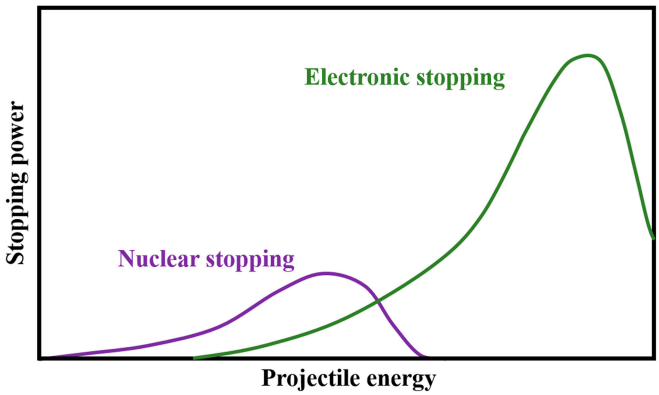

Fig. 6. A schematic representation of the nuclear (purple) and electronic (green) stopping power as a function of the ion projectile energy.

The nuclear stopping power is obtained through integration over impact parameters,

$$S_n = \int_0^\infty T(p, E_{\mathrm{CMS}}) 2\pi p \mathrm{d}p \tag{4}$$

Critical to these calculations is the selection of appropriate interatomic potentials. Early models employed screened Coulomb potentials, such as the Thomas–Fermi formulation [38,39],

$$V(r) = \phi\left(r/a_{\mathrm{S}}\right)\frac{Z_1 Z_2 \mathrm{e}^2}{r} \tag{5}$$

where Z_1 and Z_2 are the atomic numbers of the colliding pair, and $\phi\left(r/a_{\mathrm{S}}\right)$ is the scattering potential with a screening length a_{S}. Subsequently, several models, including the Bohr potential [40], Lenz–Jensen potential [41], Molière potential [42], and Ziegler–Biersack–Littmark (ZBL) potential [43], have been proposed to describe screening effects:

$$\phi\left(\frac{r}{a_U}\right) = \sum_{i=1}^{4} \alpha_i \mathrm{e}^{-\frac{\beta_i r}{a_U}} \tag{6}$$

where coefficients $(\alpha_i, \beta_i) = (0.1818, 3.2), (0.5099, 0.9423), (0.2802, 0.4028), (0.02817, 0.2016)$, and screening length $a_U = \frac{0.8853 a_0}{Z_1^{0.23} + Z_2^{0.23}}$.

Electronic stopping mechanisms model the complex electron–phonon interaction phenomena. It is typically formulated by the Bethe–Bloch formula in the case of high energies [44].

$$-\frac{\mathrm{d}E}{\mathrm{d}x} = \frac{4\pi}{m_{\mathrm{e}} c^2}\frac{n z^2}{\beta^2}\left(\frac{e^2}{4\pi\epsilon_0}\right)^2\left[\ln\left(\frac{2 m_{\mathrm{e}} c^2 \beta^2}{I\left(1-\beta^2\right)}\right) - \beta^2\right] \tag{7}$$

where β is the vacuum permittivity, e is the electron charge, m_{e} is the electron mass, and z is the point charge. n represents atomic density, $n = N_{\mathrm{a}} Z\rho / A M_{\mathrm{u}}$ (N_{a} is Avogadro's number, Z is the atomic number, ρ is the material density, A is the relative atomic mass, and M_{u} is the molar mass constant), and I is the excitation potential. Semi-empirical models have been proposed to explain electronic stopping by correlating it with equivalent proton stopping [45,46].

$$S_{\mathrm{e}}\left(Z_{\mathrm{p}}, v_{\mathrm{p}}\right) = \left(Z_{\mathrm{p}}^{\mathrm{eff}}\right)^2 S_{\mathrm{e}}\left(\mathrm{proton}, v_{\mathrm{p}}\right) \tag{8}$$

where Z_{p} is the nuclear charge, $Z_{\mathrm{p}}^{\mathrm{eff}}$ is the effective charge, and $S_{\mathrm{e}}\left(\mathrm{proton}, v_{\mathrm{p}}\right)$ is the proton stopping power, which can be obtained experimentally. Brandt and Kitagawa [47] proposed an effective method for calculating the effective charge. Thus, the ZBL stopping model is considered the most suitable for describing electronic stopping [43].

For HCIs, accurate determination of stopping power necessitates simultaneous consideration of nuclear and electronic energy loss mechanisms. At high kinetic energy, first-order perturbation theory [48] is used to describe the dependence of stopping power on the charge state of the HCIs, taking into account charge exchange, excitation, and ionization processes. Based on this approach, theoretical and experimental studies have predicted substantial enhancements in kinetic energy loss [49,50]. For HCIs with low kinetic energy, a modified electrostatic screening potential model [51] has been developed to calculate nuclear and electronic energy losses. This model demonstrates strong enhancements in nuclear and electronic stopping for slow HCIs.

Analytical potential MD (APMD) provides a simulation framework. It formulates the atoms movement using Newton's motion equations. The forces onto atoms are determined by predefined analytical potentials. They are typically expressed as:

$$V = V_{\mathrm{ext}} + V_{2\text{–body}} + V_{3\text{–body}} \tag{9}$$

where V_{ext} represents an external potential, and $V_{2\text{-body}} + V_{3\text{-body}}$ represent 2-body and 3-body interatomic potentials, respectively. For typical interatomic distances, Stillinger–Weber [52] or Tersoff [53] potentials are able to describe atomic interactions in 2DMs. However, during ion impacts, extreme compression generates interatomic separations below the cutoff radii of standard potentials. To address this, hybrid potential models are constructed by smoothly interpolating between short-range repulsive potentials (e.g., ZBL [43]) and material-specific analytical functions at larger distances. Recent advancements include ML potentials [54,55], which bypass analytical approximations by learning force fields directly from training data.

MD simulations

Classical MD has become a cornerstone technique for studying radiation damage dynamics at nanoscale spatial resolution and femtosecond temporal precision. Over 3 decades, this approach has enabled fundamental insights into ion–solid interactions through collision cascade simulations [56,57]. In 2DMs, radiation effects are modeled by imparting kinetic energy to a primary knock-on atom (PKA), initiating a sequence of atomic collisions. The PKA propagates through the lattice, displacing neighboring atoms and generating secondary PKAs until energies fall below the displacement threshold. This process creates a molten zone with liquid-like structure embedded in the crystalline matrix. Subsequent cooling via phonon diffusion leads to recrystallization, often leaving residual defects such as vacancies, interstitials, and dislocation loops. Collision cascade simulations have been pivotal in elucidating radiation damage mechanisms.

As early as 2010, Lehtinen et al. [58] utilized MD simulations to demonstrate the ion irradiation-induced formation of specific defect types in monolayer graphene. Their study systematically investigated ion species encompassing He, Ne, Ar, Kr, Xe, and Ga, with ion energies ranging from tens of eV to 10 MeV and impact angles from 0° to 88°. The resulting insights provided a

foundational framework for graphene cutting and patterning via tailored ion-type selection. Subsequently, Wu and Zhu [59] systematically investigated the effects of Ar ion irradiation on graphene/MoS_2 heterostructures with and without a SiO_2 substrate using MD simulations (Fig. 7). A hybrid potential strategy was adopted to model interatomic interactions, integrating the second-generation reactive empirical bond order (REBO), adaptive intermolecular reactive bond order, Tersoff, ZBL, and Lennard–Jones potentials. Defect generation was characterized by systematically varying irradiation energy, dose, stacking order, and substrate presence. The low-energy ion irradiation induces top-layer 2DMs to shield the bottom layer from direct damage, whereas high-energy irradiation enhances indirect collision effects via the top layer, amplifying damage in the underlying material. Conversely, the bottom-layer 2DMs consistently mitigate defect formation in the top layer, irrespective of ion energy. The substrate reinforces irradiation effects through 2 distinct mechanisms: weakened interlayer coupling at low ion energies and indirect collision cascades at high ion energies. These results offer critical support for selecting ion irradiation methods in tailoring the properties of 2D van der Waals (vdW) heterostructures. Chen et al. [60] employed MD simulations to model irradiation damage effects of intense cosmic rays on fixed-point indium (In). The study comprised 2 stages: first, a fixed-point In-graphite crucible model was designed to encapsulate high-purity In, with cosmic ray irradiation simulated across 6 dose levels (0, 99.5, 199, 298, 398, and 597 Gy) using Monte Carlo N-Particle software [61] to characterize energy deposition and high-energy proton distribution in the crucible. Second, a radiation cascade MD model was constructed, with 4 crystallographic directions (⟨001⟩, ⟨100⟩, ⟨110⟩, and ⟨135⟩) selected as PKA emission directions. Ten trajectory simulations per direction were performed for statistical robustness, with PKAs initialized at specified kinetic energies, integration steps, and emission directions, and the entire cascade collision process simulated using the microcanonical ensemble.

However, this approach encounters inherent limitations. Classical MD neglects electron dynamics, restricting their applicability to radiation types dominated by nuclear interactions (e.g., low-energy ions). Indeed, certain irradiation modalities, e.g.,

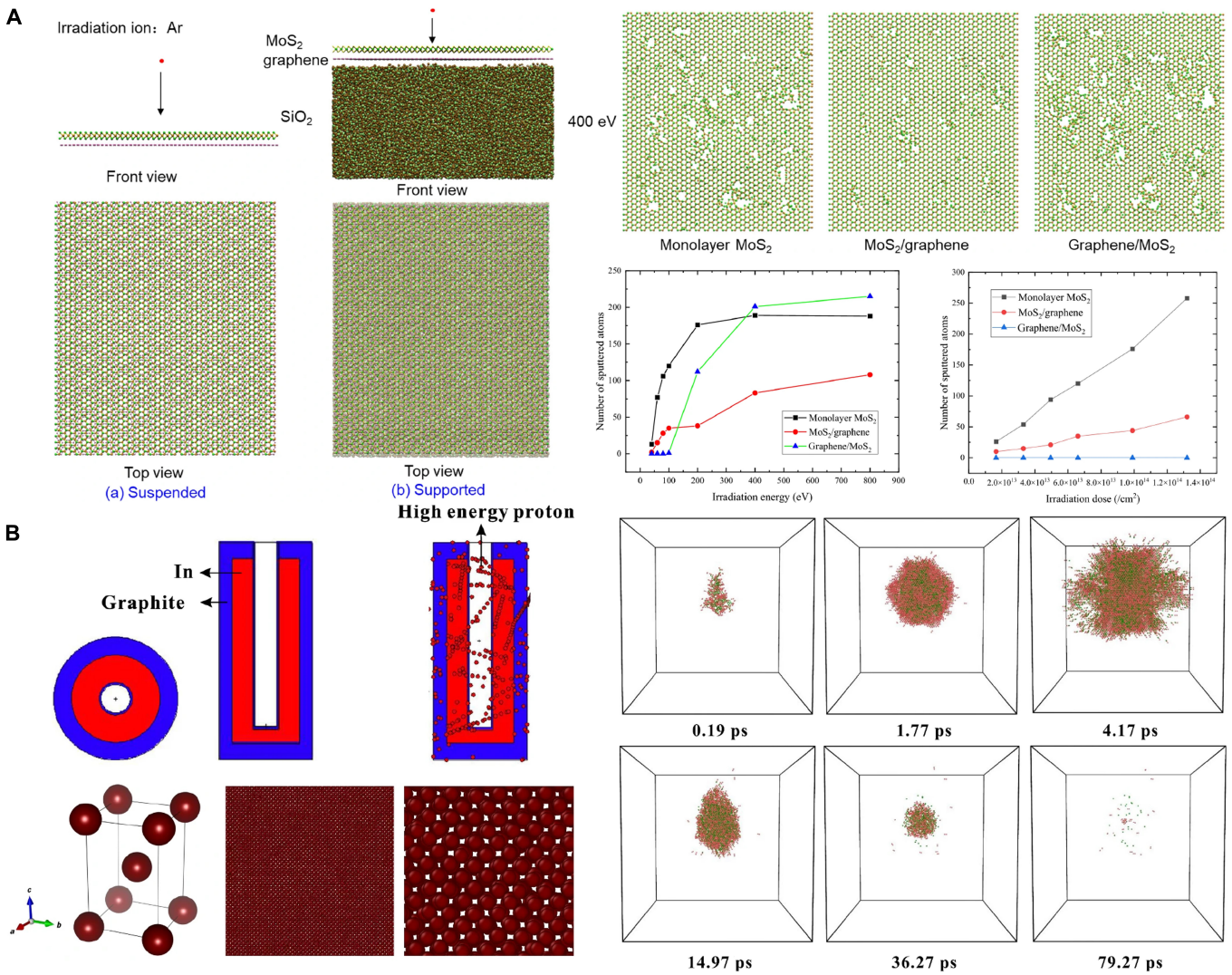

Fig. 7. (A) Schematic of the simulation model for suspended and supported MoS_2. Dependence of the number of sputtered atoms in MoS_2 layer on irradiation energy for 3 study cases. The irradiation dose is 6.6×10^{13} cm^{-2} [59]. (B) Simulation model of a prone and orthophoto of cell structure of In. Evolution of the FP number with time during the PKA cascade collision of the 10-keV kinetic energy in the metal In [60].

laser excitation, cannot be captured by classical MD. Similarly, SHIs exhibit strong electronic stopping power, necessitating quantum mechanical treatment of charge carrier interactions. As ions traverse matter, they undergo continuous energy dissipation, characterized by stopping power—the energy loss per unit path length. This process involves 2 competing mechanisms of nuclear stopping and electronic stopping. The relative dominance of these mechanisms depends critically on ion velocity. For low-energy ions ($E < 1$ MeV/u), nuclear stopping prevails, whereas electronic stopping dominates at relativistic velocities ($E > 1$ GeV/u). Intermediate regimes require hybrid models combining classical MD with quantum transport simulations to resolve electron–hole plasma formation and relaxation dynamics.

2T-MD simulations

As illustrated in Fig. 6, the proportion of energy lost via inelastic electron scattering increases notably when ions traverse solids with reduced nuclear collision cross-sections [62–64]. While modern implementations partially address electronic stopping effects by introducing friction terms into the MD equations of motion, these classical approaches fundamentally treat energy dissipated through electronic stopping as irreversible system losses. Consequently, they fail to account for electron energy transport and redistribution—precisely the limitations that the 2-temperature MD (2T-MD) framework aims to resolve.

Nonequilibrium dynamics and the 2-temperature model (2TM)

High-energy radiation events typically drive electronic subsystems far from equilibrium. Within femtosecond timescales postirradiation, electrons thermalize to a defined temperature (T_e), distinct from the lattice temperature (T_l). Subsequent picosecond-scale evolution leads to thermal equilibrium between electrons and nuclei. This transient regime is quantitatively described by coupled thermal diffusion equations in the 2TM framework [65].

$$C_e \frac{\partial T_e}{\partial t} = \nabla\left(\kappa_e \nabla T_e\right) - G\left(T_e - T_l\right) + A \tag{10}$$

$$C_l \frac{\partial T_l}{\partial t} = \nabla\left(\kappa_l \nabla T_l\right) - G\left(T_e - T_l\right) \tag{11}$$

Here, A represents the spatiotemporal energy deposition to electrons, while G, C_e, C_l, κ_e, and κ_l denote the electron–phonon coupling constant, electronic/lattice heat capacities, and thermal conductivities, respectively. Temperature-dependent material parameters introduce critical nonlinearities into this system.

Hybrid 2T-MD

The 2T-MD methodology synergizes MD and 2TM by replacing the lattice thermal diffusion equation with MD equations of motion, enabling explicit simulation of energy exchange mechanisms. Drawing inspiration from Caro and Victoria's approach [62], this framework incorporates a Langevin thermostat for energy transfer of particles with a weight of m and a speed of v.

$$m\frac{\partial v}{\partial t} = F - \gamma v + \overline{F} \tag{12}$$

where $-\gamma v$ accounts for electronic stopping losses, and the stochastic force $\overline{F}$ mediates energy deposition via electron–phonon coupling.

Current applications of 2T-MD in radiation effect simulations include laser irradiation, SHI irradiation, cascade modeling, and electron-temperature-dependent potentials [66]. Shi et al. [67] employed 2T-MD simulations to study single-layer graphene supported on a SiO_2 substrate irradiated by SHI (Xe ion) irradiation (0.5 to 25 GeV). The results revealed that lower-energy ions (0.5 GeV) created ~5-nm-diameter nanopores in graphene while inducing amorphization of SiO_2 along ion tracks (Fig. 8). With increasing ion energy, both peak electron temperature and nanopore size decreased notably, with no observable damage at 25 GeV. Crucially, the coupling between the substrate and the 2DM significantly influences structural changes due to heat transfer and atomic interactions between the different material layers. The electronic heat capacity and thermal conductivity of the substrate determine the efficiency of absorbing and dissipating energy from the ion track, directly impacting the temperature evolution and final damage morphology of the graphene. This approach provides a powerful tool for studying 2DMs and layered structures under heavy ion irradiation, underscoring the importance of electronic and thermal properties in energy transfer processes.

Multiscale calculations

AIMD

By employing AIMD, higher accuracy can be achieved at the cost of increased computational complexity. In AIMD, the equations of motion are solved based on first principles without the need for empirical parameters. Due to the complexity of solving the full many-body Schrödinger equation, various approximations are necessary. Within the Born–Oppenheimer (BO) approximation, the electronic subsystem is assumed to instantaneously relax to its ground state for each new configuration of the atomic nuclei. To calculate the system's energy and the forces on atoms, the time-independent Schrödinger equation must still be solved for different atomic configurations. This task is typically accomplished using DFT, which states that all physical properties can be described by the electron density, rather than the more complex many-electron wavefunction. The forces on the nuclei are then calculated according to the Hellmann–Feynman theorem [29,30].

$$F = -\nabla_R \langle \Psi_0 | H_e | \Psi_0 \rangle \tag{13}$$

where ∇_R represents the nuclear positions, Ψ_0 is the ground-state wavefunction, and H_e is the electronic Hamiltonian.

Mei et al. [68] studied energy storage in graphite via AIMD simulations. The nonequilibrium processes of radiation damage and associated Wigner energy in graphite were modeled using 2 methods: Frenkel pair accumulation and overlapping collision cascades. Stored energy accumulation was simulated by Frenkel pair accumulation via AIMD and overlapping collision cascades combining classical MD and AIMD. The projector augmented wave (PAW) method with the Perdew–Burke–Ernzerhof generalized gradient approximation and Tkatchenko–Scheffler vdW corrections were used to calculate equilibrium properties and defect formation energies. Radiation damage simulations involved overlapping collision cascades and random Frenkel pair creation in a supercell for AIMD. The consistency between calculated and experimental results for stored energy evolution with dosage suggests that this model could advance research on damaged graphite as an energy storage medium. Mo et al. [69] systematically investigated neutron irradiation effects on AB-stacked bilayer graphene and the influence of external

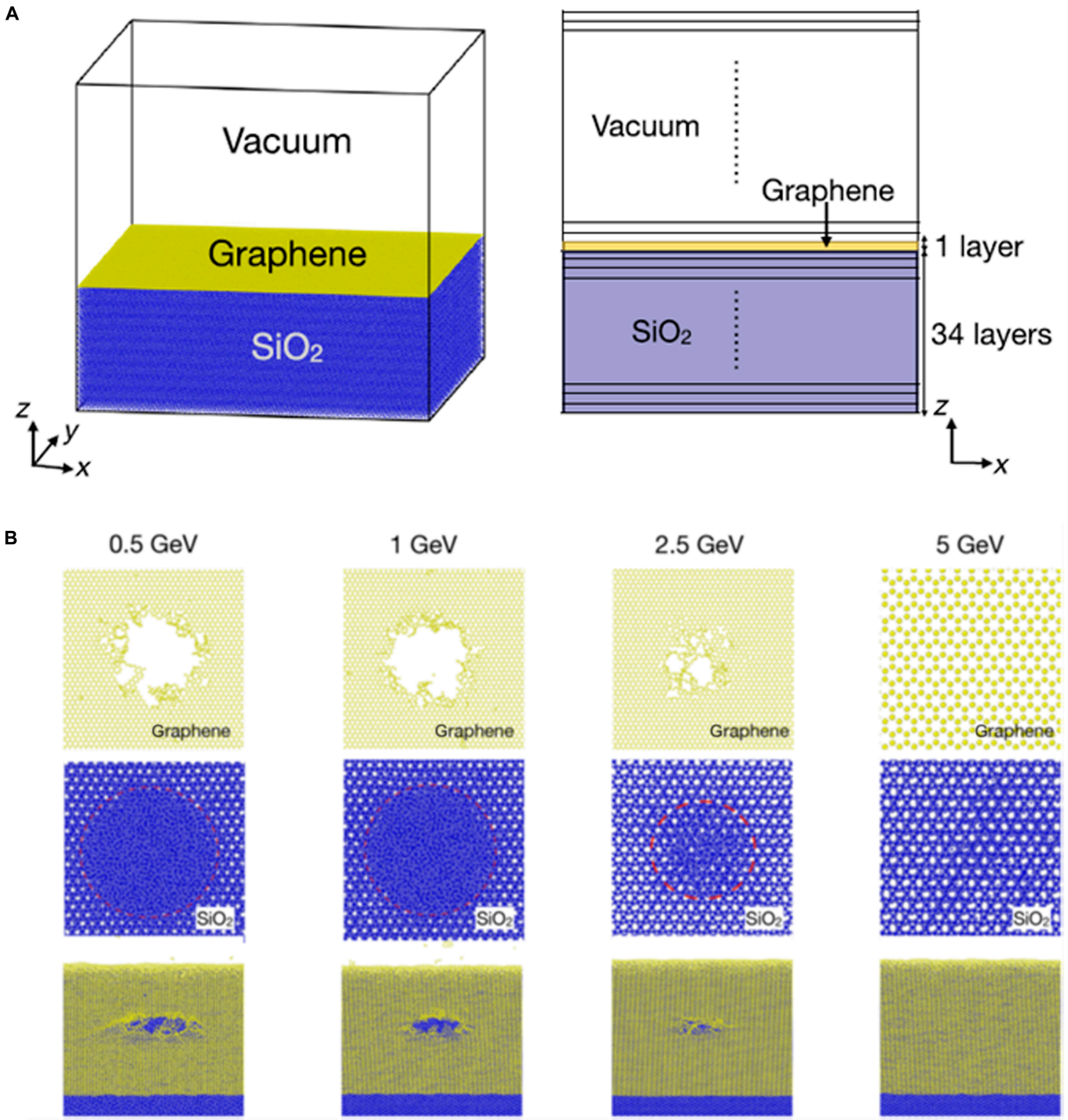

Fig. 8. (A) Simulation setup of monolayer graphene on the SiO_2 substrate. (B) Defect structures in the graphene layer and SiO_2 substrate with Xe ion energies of 0.5, 1, 2.5, and 5 GeV [67].

electric fields using DFT and AIMD with energy deposition to PKA. The results show that under constant neutron irradiation with varying electric fields, configurational changes dominate band structure evolution, with surface corrugation playing a minor role. Reducing interlayer spacing stabilizes configurations and band structures under electric fields. The Young's modulus is primarily influenced by microstructural changes and surface corrugation, with configurational effects being secondary. Electric fields can precisely modulate bandgaps under irradiation but concomitantly reduce Young's modulus, potentially impacting electrical and thermal conductivity.

DFT + MD

The ab initio BO MD describes interatomic forces with significantly higher accuracy than other atomistic methodologies. However, its application to ion impact modeling is computationally prohibitive due to the requirement of simulating numerous trajectories. To address this limitation, 2 complementary atomistic

simulation methods, including binary collision approximation (BCA) models [70] and sophisticated APMD simulations [71], can be employed to predict the optimum ion energy. These methods exhibit reasonable efficacy for bulk systems, where ions undergo multiple collisions with target atoms before coming to rest. However, their applicability to 2DMs remains debated [72,73]. The core limitation lies in their inadequate representation of chemical interactions between atoms, which become particularly critical at low ion energies [74]. Furthermore, ion transport codes and analogous frameworks typically model solid targets as amorphous structures with uniform density, a simplification that fails to capture the physics of 2DMs—where ion–target interactions often involve essentially single-collision events and rely on crystalline atomic arrangements.

Kretschmer et al. [74] utilized BO DFT-MD simulations to model ion impacts on graphene and h-BN, quantifying the threshold ion energy (E_{th_ion}) for various ion species. Their work demonstrated the inadequacy of the BCA method for many ions and emphasized the critical role of chemical interactions during ion impacts. Ma et al. [75] conducted classical MD simulations of ion-irradiated WS_2 monolayers to accurately describe ion–WS_2 interactions. To assess the effects of substrate corrugation and off-normal ion incidence on defect generation, sputtering yields were analyzed as a function of incidence angle (θ). First-principles calculations clarified the relationship between S-vacancy density and band structure of WS_2, revealing that S-vacancies introduce deep states in the bandgap, governing near-infrared optical absorption. Enhanced linear and saturated absorption in WS_2 with increasing S-vacancy density was observed and interpreted through DFT results. Kretschmer and Krasheninnikov [76] compared AIMD, APMD, and BCA models to gain insights into the interplay of chemical interactions and the collective motion of target atoms near the impact site (Fig. 9). Their findings showed that APMD provides reasonable results for inert gas atoms but overestimates the optimum ion energies for B and N implantation into graphene. This discrepancy arises from APMD's inadequate description of the energetics of complex atomic configurations, which deviate from the standard "training configuration set" used in potential parametrization. To address this, a modified BCA approach was proposed, requiring minimal input from first-principles calculations, enabling rapid determination of the optimum ion energy for implantation into 2D systems. Notably, the study demonstrated that conventional BCA and modified BCA calculations provide upper and lower bounds for the optimum ion energy across all investigated scenarios, offering a pragmatic framework for ion implantation design in nanomaterials.

Fekri et al. [77] investigated monolayer MoS_2 FETs on SiO_2 substrates irradiated with He^+ ions (5 to 7.5 keV) and observed a marked negative shift in threshold voltage and an increase in conductivity at low irradiation doses (1×10^{12} to 5×10^{12} ions/cm^2). Complementary MD simulations were employed to unravel the microscopic mechanisms of ion-induced damage, while DFT calculations analyzed the impact of impurities on the electronic structure of MoS_2. The results revealed the substrate-dependent damage generation mechanism, which was attributed to the generation and accumulation of mobile holes and electron traps within the SiO_2 dielectric layer due to ion irradiation, with these trapped charges altering the charge state at the MoS_2–SiO_2 interface. The introduction of an h-BN buffer layer reduced the threshold voltage shift, clearly demonstrating the crucial role of the substrate material in modulating the interfacial charge and electrical properties of the 2DMs. Ghorbani-Asl et al. [78] integrated APMD with DFT to investigate defect generation in freestanding MoS_2 sheets under inert gas ion irradiation across a broad energy range, where nuclear stopping dominates (Fig. 10). The ZBL potential was employed to model ion-MoS_2 interactions, with MD simulations revealing defect formation dependencies on ion energy, incidence angle, and MoS_2's layered atomic structure. DFT calculations, implemented via the Atomistix ToolKit (ATK), were used to characterize electronic structure alterations and transport property modifications induced by irradiation-induced defects. The study demonstrated the feasibility of designing hybrid MoSX compounds (where X denotes a Group V or VII chemical element) and discussed the properties of such systems and lateral MoSX-MoS_2 heterostructures.

MC method

To face the challenges from the limited calculation resources with DFT and MD approaches for investigating irradiation effects, MC software-SRIM is widely used for bulk materials [37]. However, it is not readily adaptable to 2DMs due to dimensional constraints. MD combined with DFT has been applied to simulate energetic ion impacts on suspended 2DMs [79], but becomes computationally infeasible for projectile kinetic energies exceeding 100 keV. Therefore, hybrid methods integrating DFT with MC or MD with MC have been explored for ion irradiation simulations.

As shown in Fig. 11, Li et al. [80] conducted a systematic investigation of ion irradiation effects in 2D Ti_2C using an integrated approach combining ab initio and MC simulations. Their results revealed that ion-induced defects form through primary collision events and in-plane recoil mechanisms. DFT calculations were implemented via VASP code with the PAW method and PBE functional, and characterized the structure and defect formation energies of Ti_2C. An MC framework rooted in BCA was developed to model defect creation under ion bombardment. MC simulations of ions (H, He, Li, Be, B, C, N, O, F, and Ne) and isotopes (e.g., ^1H, ^4He, and ^{12}C) at energies of 0.5 to 20 MeV showed that displaced atom counts decrease with incident energy and increase with ion atomic number. Ti atoms were more prone to displacement than C atoms during irradiation, offering potential for selective etching in electronics. Electronic structure analyses confirmed that Ti_2C maintains metallic conductivity even with large vacancy concentrations (up to 16% missing atoms), indicating robust irradiation tolerance for electrical conductivity. Subsequently, Kretschmer et al. [28] proposed a computationally efficient framework combining APMD and MC to model irradiation of supported graphene and MoS_2. This approach independently evaluates contributions to damage from backscattered ions and sputtered substrate atoms. MD simulations performed in large-scale atomic/molecular massively parallel simulator (LAMMPS) utilized modified Stillinger–Weber and ZBL potentials to describe interatomic interactions, simulating ion and substrate atom impacts on 2DMs. MC methods in TRIDYN calculated backscattering probabilities and energy/angular distributions, complementing MD results. The study revealed that defects in 2DMs primarily originate from backscattered incident ions and sputtered substrate atoms. For MoS_2 on a SiO_2 substrate irradiated with 1- to 30-keV He ions, the total sputtering yield of S atoms from sputtered substrate atoms and backscattered He ions was significantly higher (up to ~5×) than in the suspended case. Similarly, supported graphene exhibited more defects due

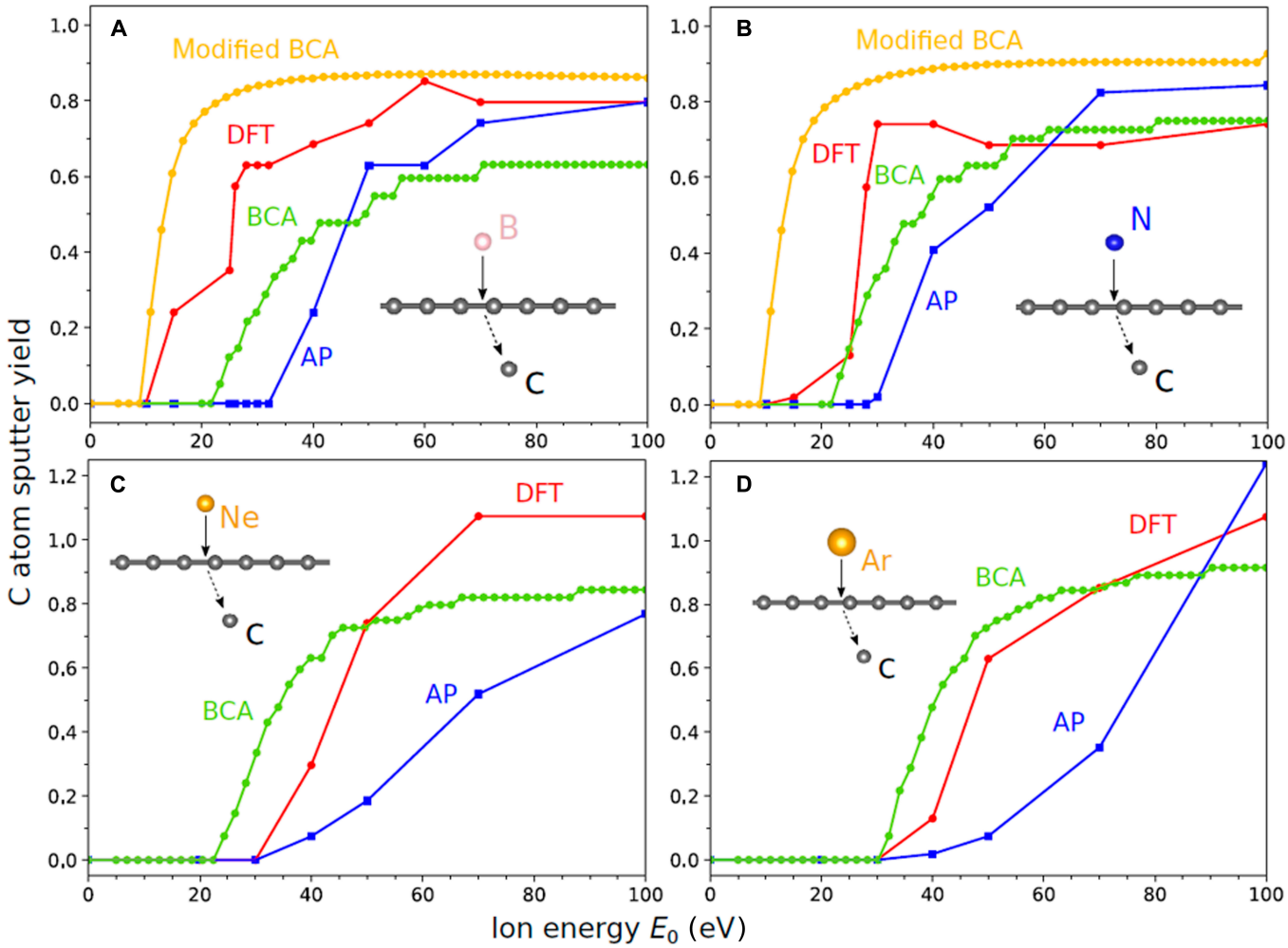

Fig. 9. Carbon atom sputtering yields calculated using AIMD (red), APMD (blue), BCA (green), and the modified BCA (yellow) scheme for B (A), N (B), Ne (C), and Ar (D) ions during low-energy ion irradiation of graphene [76].

to the action of backscattered ions. This indirect damage mechanism expands the effective range of influence of incident ions, thereby increasing the equivalent collision cross-section of the 2DMs. Li et al. [81] developed a theoretical framework, I2DM, to simulate ion irradiation on 2DMs using MC algorithms. I2DM generates incident ions with tunable ion species, incident energies, ion fluxes, and incident angles. Based on the BCA, primary collisions, cascade collisions, and defect recombination during irradiation are explicitly described. As output, I2DM provides detailed statistics on defect types, yields, and morphological changes in irradiated materials, offering a versatile tool for predictive modeling of ion–solid interactions in nanoscale systems.

TDDFT + Ehrenfest MD method

Time-dependent DFT (TDDFT) combined with Ehrenfest MD (TDDFT and Ehrenfest MD) aims to simulate real-time interactions between electrons and nuclei under external perturbations e.g., light excitation. This method allows simultaneous treatment of quantum dynamics of electrons and classical motion of nuclei, making it particularly suitable for studying nonadiabatic processes like photochemical reactions and excited-state dynamics. TDDFT can be categorized into 2 types: Linear response (LR)-TDDFT and RT-TDDFT. The LR-TDDFT is usually used for calculating the optical spectrum of a system from its electronic structure (e.g., wavefunctions and energy bands). Thus, it is not employed for dynamical simulations that produce information about the system's time evolution. In contrast, RT-TDDFT can evolve the system and enable dynamical simulations.

TDDFT is based on the Runge–Gross theorem, which simplifies the time-dependent many-electron problem to an effective single-electron potential problem. Its core equation is the time-dependent Kohn–Sham equation:

$$i\hbar\frac{\partial\psi_i(rt)}{\partial t}=\left[\frac{-\hbar^2}{(2,m)}\nabla^2+v_{\mathrm{eff}[n](r,t)}\right]\psi_{i(r,t)} \qquad (14)$$

where $\psi_{i(r,t)}$ represents the Kohn–Sham orbitals and $v_{\mathrm{eff}}[n]=v_{\mathrm{ext}}+v_{\mathrm{H}}[n]+v_{\mathrm{xc}}[n]$is the effective potential comprising external field potential, Hartree potential, and exchange-correlation potential. The electron density is given by $n(r,t)=\sum_i|\psi_{i(r,t)}|^2$. The exchange-correlation potential typically employs the adiabatic approximation.

Ehrenfest MD describes nuclear motion through classical Newton's equations, with forces determined by quantum expectation values of the electronic state, thus coupling nuclei and electrons:

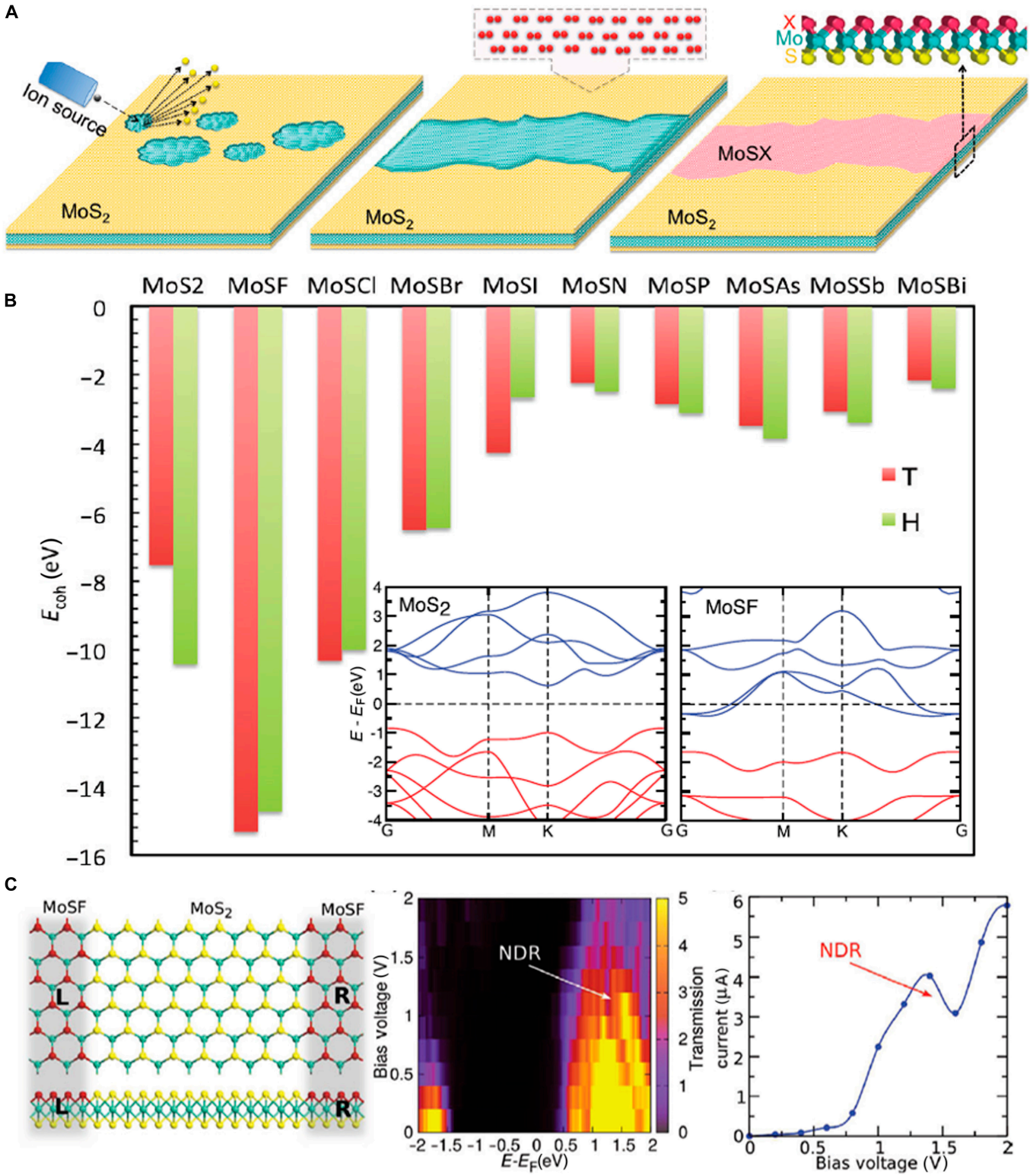

Fig. 10. (A) Schematic illustration of ion-beam-mediated production of mixed MoSX material starting from MoS_2-ML. (B) Cohesive energy per primitive cell for the MoSX alloys where X stands for chemical elements from group V and VII. (C) Schematic illustration and its bias-dependent transmission contour plot *I*–*V* characteristics of a MoSF–MoS_2–MoSF-based device [78].

$$M_{\mathrm{I}}\frac{\mathrm{d}^2R_I}{\mathrm{d}t^2} = -\nabla_{R_I}\left\langle\psi(t)|\hat{\mathrm{H}}_{\mathrm{KS}}|\psi(t)\right\rangle \tag{15}$$

where M_I and R_I are the mass and position of the Ith nucleus, and $\hat{H}_{\mathrm{KS}}$ is the Kohn–Sham Hamiltonian. Forces are calculated using the Hellmann–Feynman theorem: $F_{I(t)} = -\left\langle\psi(t)|\frac{\partial\hat{\mathrm{H}}_{\mathrm{KS}}}{\partial R_I}|\psi(t)\right\rangle$, which also considers derivatives of ion–electron interactions, Hartree potential, and exchange-correlation potential with respect to nuclear coordinates.

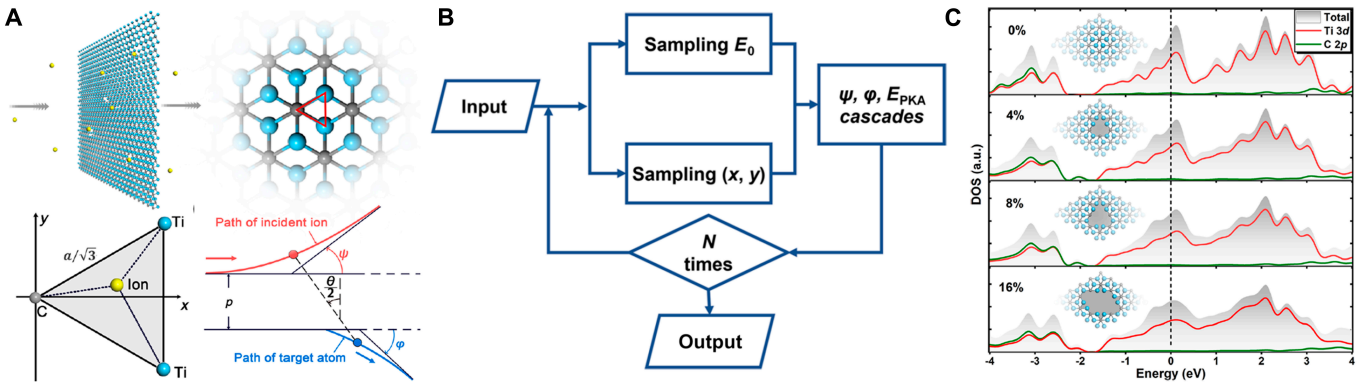

Fig. 11. (A) Schematic of energetic ion bombardment on a 2D Ti_2C sheet and the trajectories for an incident ion and a target atom interacting with a central repulsive potential. (B) Simulation flowchart of the developed MC approach. (C) Total and partial DOS projected onto the Ti 3d and C 2p orbitals for pristine and irradiated Ti_2C sheets with vacancies (reprinted [adapted] with permission from Ref. [80]; Copyright 2023, American Chemical Society).

The computational workflow of the TDDFT Ehrenfest MD method is shown in Fig. 12. It begins with ground-state DFT, first optimizing ionic positions R_I through energy functional minimization $\left(min_{R_I} E_{\mathrm{DFT}}[\rho, R_I]\right)$ and solving the ground-state Kohn–Sham equations $\left(\hat{H}_{\mathrm{KS}}\psi_i = \varepsilon_i \psi_i\right)$ to obtain equilibrium electron density $\rho(r)$ and corresponding Kohn–Sham orbitals $\psi_i^{\mathrm{GS}(r)}$. Time evolution conditions are then initialized: electronic wavefunctions are set to ground-state solutions $\left(\psi_{i(r,0)} = \psi_i^{\mathrm{GS}(r)}\right)$, while ionic positions $R_{I(0)}$ and velocities $\dot{R}_{I(0)}$ are configured according to the physical scenario (e.g., thermal motion or external excitation). The time-stepping cycle then alternately updates electronic and ionic degrees of freedom:

1. Electronic evolution: Based on the time-dependent Kohn–Sham equation $\left[i\partial_t \psi_i(r,t) = \hat{H}_{\mathrm{KS}}[\rho(t)]\psi_i\right]$, electronic wavefunctions are propagated to the next time step $\left[\psi_i(r, t+\Delta t) \approx \mathrm{e}^{\left(-i\hat{H}_{\mathrm{KS}}\Delta t\right)}\psi_i(t)\right]$ using numerical methods, e.g., Crank–Nicolson, and instantaneous electron density $\rho(r, t)$ is calculated;
2. Ionic force calculation: According to Ehrenfest's theorem, quantum mechanical forces on each ion are computed using the Hellmann–Feynman formula $(F_I(t) = -\int \rho(r,t)\frac{\partial V_{\mathrm{ext}}(\boldsymbol{r},(\mathbf{R})_I)}{\partial R_I}$, with Coulomb repulsion between ions added;
3. Ionic motion update: Ionic motion is driven by Newton's equation $\left(M_I R_I = F_I^{\mathrm{total}}(t)\right)$ with positions and velocities updated using the velocity-Verlet algorithm $R_I(t+\Delta t) = R_I(t) + v_I(t)\Delta t + \frac{F_I^{\mathrm{total}}(t)}{2M_I}\Delta(t)^2$.

This cycle repeats with coordinated time steps (typically 0.1 to 1 fs) until reaching the preset total simulation time. The final output includes ionic trajectories $R_I(t)$ and electronic dynamic properties (e.g., excited state populations and transient dipole moments), fully characterizing the system's real-time evolution under nonadiabatic coupling. This workflow couples electronic and ionic dynamics through mean-field approximation, suitable for modeling nonequilibrium quantum dynamics processes like ultrafast laser excitation and molecular photodissociation, with computational efficiency limited by the high-frequency Kohn–Sham equation solutions in TDDFT.

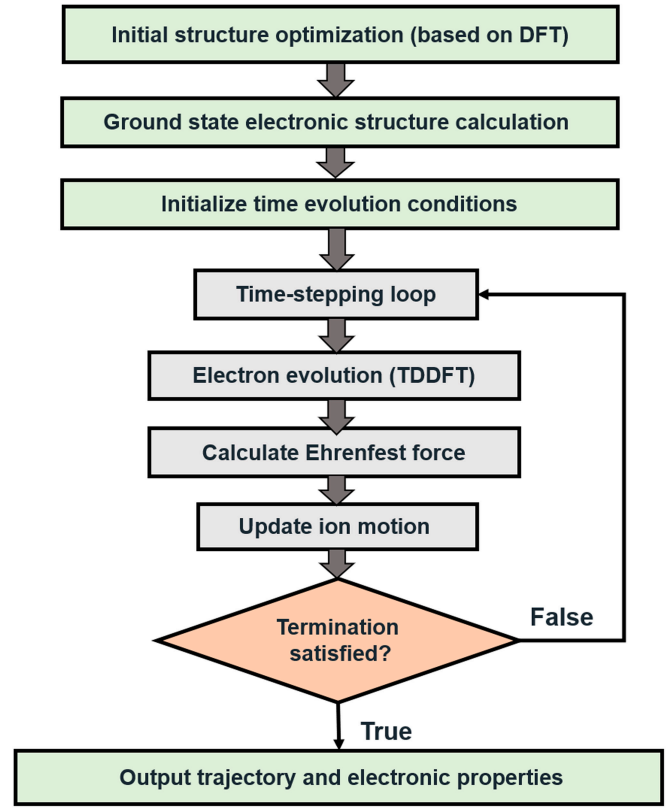

Fig. 12. TDDFT calculation flowchart.

As depicted in Fig. 13A, Ojanperä et al. [82] developed a computational framework integrating TDDFT with Ehrenfest MD, incorporating PAW pseudopotentials to explicitly model core electron contributions. This approach enabled the first-principles calculations of electronic stopping power (S_e) for high-energy ions (H^+, He^{2+}) in graphite targets across the full energy range (3 keV to 2 MeV). The study elucidated that core electron excitations make a significant contribution to S_e in the MeV energy regime (reaching up to 30% for He^{2+}) and validated the velocity matching effect, with the S_e peak occurring at 150 keV in close agreement with experimental observations.

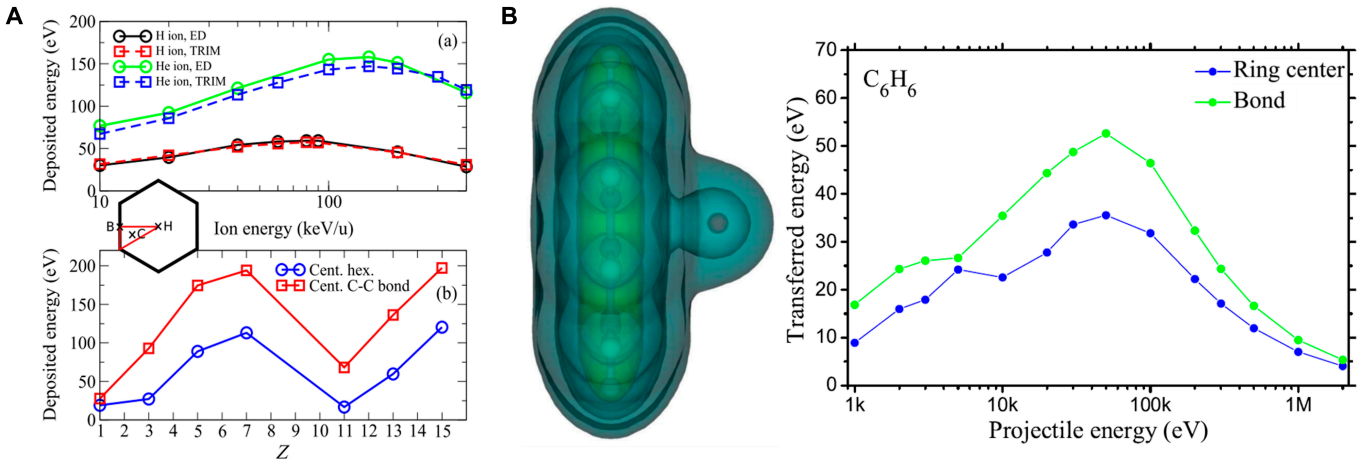

Fig. 13. (A) Energy deposited into the graphene target for H and He ions as a function of initial projectile energy [82]. (B) Total energy transferred to a graphene fragment as a function of proton energy [83].

Additionally, multilayer graphite was found to exhibit a 15% increase in S_e due to enhanced electronic excitation channels from interlayer interactions. Bubin et al. [83] combined TDDFT and Ehrenfest MD to systematically study collision dynamics between H^+ and He^{2+} with graphene fragments. The research employed the local density approximation functional and Troullier–Martins pseudopotentials, simulating the coupling of electronic excitation and nuclear motion in real-space finite-difference grids. It revealed that in proton collisions, the energy transfer peak occurs at 30 keV with over 90% dissipated through electronic excitation, yet no C–C bond breaking was observed even at energies up to 2 MeV. In contrast, highly charged He^{2+} achieved energy transfers of 150 eV at 50 keV, directly inducing bond breaking in benzene molecules. Trajectory analysis further revealed that energy transfer efficiency increases by 20% when ions pass through C–C bonds rather than through the center of hexagonal rings, attributed to enhanced Coulomb interactions due to higher electron density in bond regions. Kretschmer and Krasheninnikov [84] employed TDDFT and Ehrenfest MD to investigate the microscopic mechanisms of defect formation in 2DMs during ion irradiation. They implemented the simulations in the GPAW code [85] and utilized a real-space grid (spacing 0.2 Å) with the PBE exchange-correlation functional and PAW method. The researchers modeled various 2DMs including graphene, hexagonal boron nitride (h-BN), and TMDs, using supercells containing 50 to 200 atoms with periodic boundary conditions. For ion irradiation, they simulated He^+, Ne^+, Ar^+, and Xe^+ ions with energies ranging from 100 eV to 10 keV, tracking both electronic excitations and nuclear collisions with femtosecond time resolution.

The TDDFT + Ehrenfest MD method offers distinct advantages over traditional approaches. Unlike classical MD with empirical potentials, it explicitly incorporates electronic excitations and describes bond breaking/formation via quantum mechanical principles. Compared to BCA methods, which dominate radiation damage simulations, this approach provides time-resolved insights into electronic dynamics and captures collective many-body effects. However, its semiclassical mean-field treatment of electron-ion interactions may inadequately describe nonadiabatic transitions between electronic states, particularly at low ion velocities. Additionally, the computational cost scales unfavorably with system size, typically restricting simulations to sub-1,000 atom systems and picosecond timescales. Notwithstanding these limitations, TDDFT + Ehrenfest MD represents a state-of-the-art framework for studying atomistic processes during ion irradiation. Its ab initio nature makes it uniquely suited for novel 2DMs, where empirical potentials often lack transferability. Recent advancements in exchange-correlation functionals, nonadiabatic dynamics formalisms, and parallel computing have expanded its applicability to more complex materials systems. As these methodologies continue to evolve, they hold marked promise for unraveling the intricate interplay between electronic excitations and nuclear motion in radiation environments, ultimately enabling predictive design of radiation-hardened 2DMs-based devices.

FEA methods

Due to continuous radiation exposure, electronic components may suffer from ionization damage. Extensive studies on the effects of irradiation on GFETs have been conducted [86–88], yielding notable progress. It revealed that molecular adsorption [89–91], charge accumulation in gate oxides [92–94], or radiation-induced defects [95,96] in graphene can impair device electrical properties. However, it is difficult to obtain device-level damage results quickly through atomic-level simulation, and therefore, solutions and predictions need to be made through FEA methods [97].

Current FEA of 2D semiconductor (e.g., MoS_2) devices remains challenging because bulk-based parameter descriptions cannot accurately capture layered spatial charge distributions and 2D DOS, despite requiring thickness-specific material parameters [98–100]. To address this, Donetti et al. [101] modeled the layered structure of MoS_2 using a stack of alternating semiconductor and insulating layers representing vdW gaps [102]. Material parameters were extracted directly from DFT calculations. By analyzing charge distributions in mono- and few-layer structures under out-of-plane electric fields, they derived a layered dielectric model and extracted layer-dependent N_c and N_v values from full DOS calculations. Technology computer-aided design (TCAD) simulations comparing this layered model with a uniform model using averaged parameters demonstrated discrepancies in capacitance calculations for metal-oxide-semiconductor structures, highlighting the importance of layered descriptions in accurately predicting device

behavior. Investigating the total dose effect on GFETs under various biases and doses is critical, as bias conditions and doses are primary determinants of radiation response [103,104]. Li et al. [105] systematically studied the TID effects of 10 keV x-ray irradiation on GFETs with varying structures and dimensions (Fig. 14). Using TCAD simulations, they modeled the impact of radiation-induced oxide trap charges in the gate oxide of top-gate devices on radiation response. Results showed that Dirac voltage V_{Dirac} and carrier mobility (μ) degraded progressively with increasing dose. Top-gate GFETs exhibited more severe radiation damage compared to back-gate configurations, and the dose effect on device performance depended on structural dimensions.

ML-Driven Multiscale Simulations of Radiation Effects in 2DMs

Artificial intelligence and ML are revolutionizing the study of radiation response in 2DMs by enabling data-driven insights into complex atomic and electronic processes [106–108]. These techniques address critical challenges in traditional simulation approaches, such as limited spatiotemporal resolution and reliance on empirical approximations.

Currently, ML interatomic potentials (MLIPs), including Gaussian approximation potentials and neural network potentials, offer remarkble advantages for simulating radiation-induced defect formation [54,109,110]. Table 3 compares the

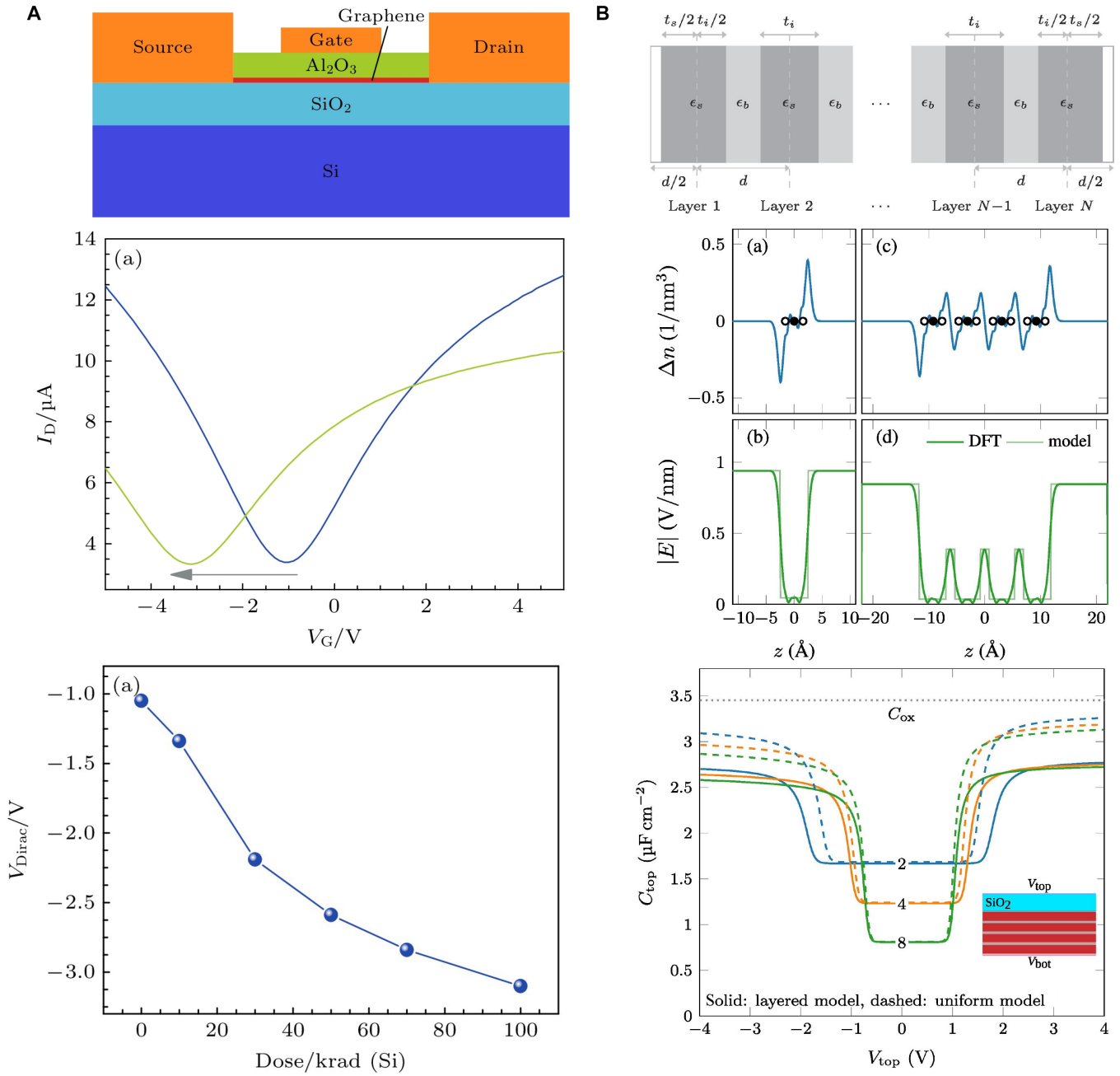

Fig. 14. (A) Transfer characteristic curve and the variations of V_{Dirac} with cumulative dose shift as functions of the total dose of a top-gate graphene field effect transistor [105]. (B) Excess electron density Δn and electric field E for MoS_2 with 2 V bias calculated with layered model for MoS_2. Capacitance of the structure depicted in the inset obtained with TCAD simulations [101].

strengths and weaknesses of traditional and MLIPs, some of which are complementary. When constrained to their validated configurational space, MLIPs can achieve energy and force predictions with DFT-level accuracy (sub-meV/atom), while enabling orders of magnitude computational acceleration over first-principles methods. Their linear scaling with system size makes them uniquely suited for simulating radiation damage dynamics in large-scale 2D material systems. However, MLIPs suffer from limited extrapolation capability to uncharted structural regimes, particularly under extreme conditions like ion irradiation. To address this, physics-informed ML potentials integrate physical constraints (e.g., conservation laws and symmetry principles) with data-driven regression, preserving DFT-level fidelity while maintaining computational efficiency. These hybrid frameworks retain the interpretability of classical potentials and eliminate overfitting artifacts, thus extending predictive capabilities to nontrivial scenarios encountered in radiation environments. Guo et al. [111] used the small-data-based MLIPs to model defect migration in graphene under proton bombardment, revealing previously unobserved vacancy clustering dynamics. This approach bridges the gap between computationally intensive ab initio methods and classical MD simulations, enabling large-scale studies of radiation damage in 2DMs. Mishin et al. [112,113] developed improved physics-informed neural network (PINN) potentials for Al and Ta by training on a large database of electronic structure calculations and accurately predicted a variety of physical properties, e.g., thermal expansion, energies of point and extended defects, melting temperatures, and structural and kinetic properties of liquid aluminum (Fig. 15).

Zheng and Gu [114] employed the kernel ridge regression (KRR) algorithm to uncover latent correlations between defect sites and thermal vibration patterns. The KRR model, trained on thousands of thermal vibration morphologies generated via MD simulations, demonstrated robust capability in detecting uniformly distributed defects in graphene (Fig. 16A). Results indicated that the atomistic strategy enabled accurate prediction of single-atomic vacancies, while the domain-based method successfully identified multiple vacancies with unknown stoichiometry. They achieved approximately 90% prediction accuracy on held-out test datasets, underscoring the efficacy of ML frameworks in defect analysis for 2DMs. Jinnouchi et al. [115] developed an efficient real-time MLFFs method integrated into an electronic structure code. Rooted in Bayesian inference during MD simulations, this approach automatically generates MLFFs by performing first-principles calculations only for new atomic configurations sampled during simulations. This adaptive strategy enables rapid construction of a first-principles dataset across broad phase spaces while maintaining high simulation throughput.

In 2023, Dash et al. [116] observed the formation of defects in monolayer MoS_2 under electron irradiation with an ultralow

Table 3. Comparison of 3 classes of interatomic potentials [54,109]

	Traditional	ML	Physically informed ML
Physical foundation	Strong	None	Strong
Number of fitting parameters	~10	>1,000	>1,000
Computational speed	Very high	Slower	Slower
Reference database	Small	Large	Large
Accuracy (interpolation)	Limited	~1 meV/atom	~1 meV/atom
Transferability	Reasonable	Poor	Reasonable
Reliance on human expertise	Strong	Weaker	Weaker
Extension to chemistries	Challenge	Challenge	Challenge
Systematically improvable	No	Yes	Yes

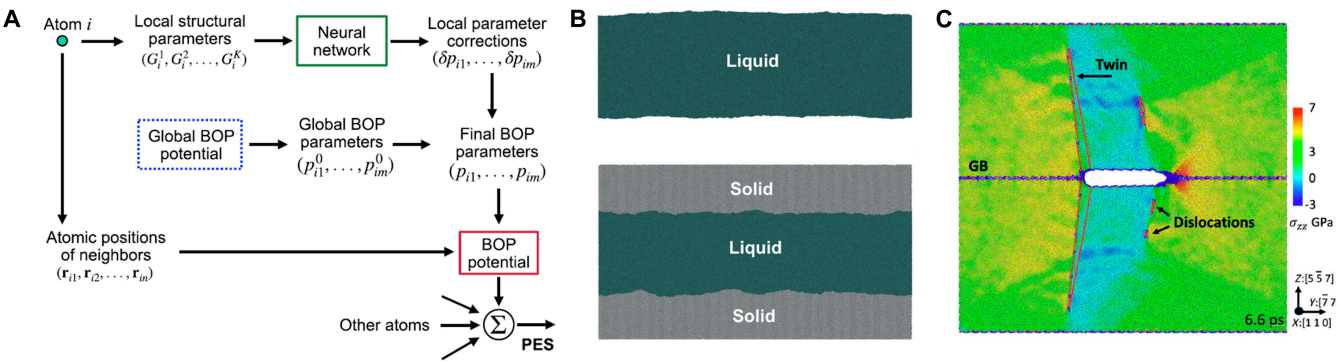

Fig. 15. (A) Flowchart of the modified PINN method. (B) Simulation blocks used for computing the interface tensions in Al. (C) MD simulation of crack nucleation and growth on a [1 1 0] symmetrical tilt boundary in Al performed with the PINN Al potential [112].

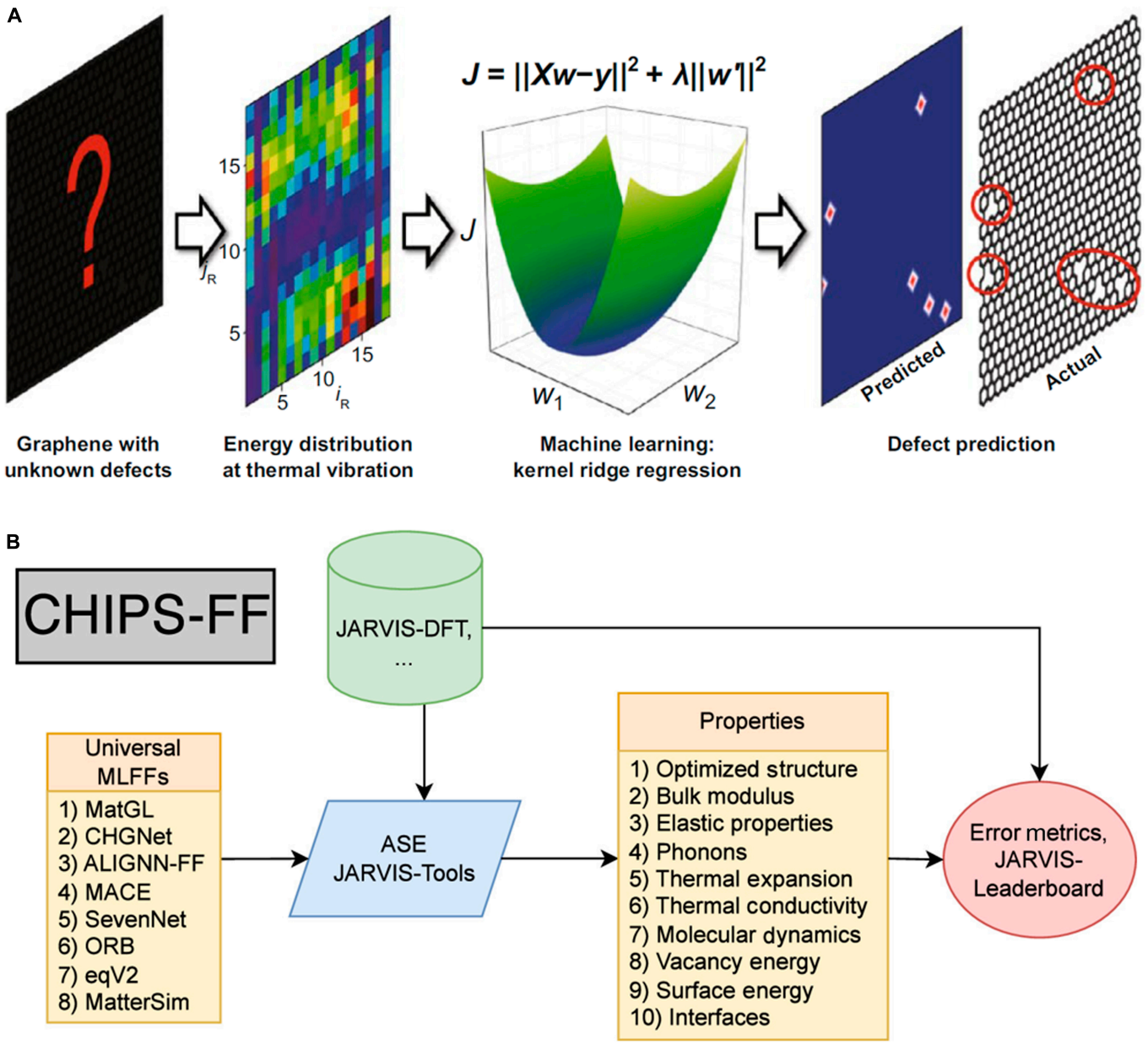

Fig. 16. (A) Flowchart of machine learning-based detection of graphene defects with atomic precision [114]. (B) A full schematic of the CHIPS-FF workflow [117].

acceleration voltage (≤5 keV). At the same time, with the increase of the electron dose, an overall quenching of the PL intensity occurred, and defect peaks appeared in the Raman spectrum. By combining DFT and MLFFs to simulate the Raman spectra of MoS_2 with defect distributions, the study confirmed that sulfur vacancies represent the dominant defect type. Recently, Wines and Choudhary [117] developed CHIPS-FF (Computational High-Performance Infrastructure for Predictive Simulation-based Force Fields), an open-source benchmarking platform for MLFFs. This platform utilized 16 graph-based MLFFs including ALIGNN-FF, CHGNet, MatGL, MACE, SevenNet, ORB, MatterSim, and OMat24; CHIPS-FF integrates the Atomic Simulation Environment with JARVIS-Tools to facilitate high-throughput simulations (Fig. 16B). It streamlines the evaluation of MLFF accuracy and computational efficiency across diverse 2DM systems, advancing data-driven force field development for nanoscale materials modeling.

Conclusion and Prospects

Conclusion

2DMs exhibit unprecedented potential for radiation-intensive applications in aerospace and nuclear systems, yet their operational reliability under ionizing radiation remains a critical challenge. Multiscale computational modeling has emerged as a transformative tool to address this challenge by integrating atomistic simulations (DFT/MD), mesoscale transport models (MC), and ML frameworks. Key advancements include the following:

Synergy of multiscale methods

Combining DFT, MD, MC, and ML, it can successfully reveal the defect evolution mechanisms (e.g., vacancy formation and doping effects), energy transfer pathways (nuclear blocking vs. electron blocking competition), and structure–performance relationships of 2DMs under ion irradiation. DFT calculations of defect

formation energies, MD simulations of collisional cascade processes, and ML-accelerated potential field construction have collectively advanced the atomic-level understanding of irradiation damage.

Accurate description of electronic excitation and thermal effects

By introducing 2T-MD and TDDFT, quantitative analyses of electron–phonon coupling effects have been achieved, breaking through the limitations of conventional MD that only considers nuclear interactions. This advancement provides a theoretical tool to explain the electron-excitation-dominated damage under the irradiation of high-energy ions (e.g., SHI).

Combination of data-driven and experimental validation

ML models based on high-throughput computational and experimental data have significantly improved the defect prediction efficiency (e.g., the effect of sulfur vacancies on the Raman spectra of MoS_2) and provided a "computational-experimental" closed-loop optimization pathway for the design of novel 2DMs.

Prospects

Adaptive multiscale integration

Develop hybrid algorithms that dynamically couple electronic structure calculations (e.g., TDDFT) with mesoscopic phase-field models to resolve defect evolution across 10^{-18} to 10^{-6} s and 10^{-10} to 10^{-6} m. Advance 2T-MD simulations using implicit time integrators and graphics processing unit (GPU)-accelerated solvers to enable 3-dimensional modeling of electron–hole plasma formation and thermal diffusion in irradiated 2DMs.

ML-driven efficiency revolution

Replace classical potentials with PINN potentials for large-scale MD simulations of defect migration and doping dynamics in 2DMs. Construct comprehensive radiation damage databases incorporating defect formation energies, displacement thresholds, and carrier mobility degradation rates to train ML models for rapid material screening.

Quantum mechanical refinement

Implement nonadiabatic dynamics methods (e.g., surface hopping TDDFT) to accurately describe electronic state transitions during ion–solid interactions, overcoming BO approximations. Apply quantum MC and GW-BSE calculations to resolve electron–hole pair generation and recombination kinetics in irradiated 2DMs.

Application-specific toolchains

Develop multiscale simulation platforms for evaluating 2D heterostructures under combined irradiation, thermal cycling, and mechanical stress, leveraging phase-field models to predict long-term device degradation. Integrate in situ characterization techniques (e.g., scanning transmission electron microscopy [STEM]-electron energy loss spectroscopy [EELS]) with computational models to validate electronic temperature distributions and defect configurations in real time.

Overall, the challenge lies in creating a unified "predict–design–validate" framework that merges atomistic physics, ML-driven data analytics, and experimental validation. By fostering interdisciplinary collaboration across computational science, materials engineering, and radiation physics, researchers can unlock the full potential of 2DMs in extreme radiation environments. This breakthrough will revolutionize radiation-hardened electronics for deep-space exploration, advanced nuclear reactors, and next-generation sensing systems.

Acknowledgments

Funding: This work was financially supported by the State Key Laboratory of Luminescence Science and Technology (Grant No. SKLA-2024-04) and the Shanghai Research Center for Silicon Carbide Power Devices Engineering and Technology Project (Grant No. 19DZ2253400).
Author contributions: H.T. designed this study. H.T. and Z.C. wrote the manuscript. H.T., Z.C., M.T., N.Y., and W.S. collectively conducted the literature review. L.M., J.F., R.Z., and G.Z. provided suggestions and revised the manuscript through various versions.
Competing interests: The authors declare that they have no competing interests.

Data Availability

There are no data associated with this article.

References

1. Wang S, Wang Q. 2D materials for space use. In: *Two-dimensional materials for nonlinear optics*. Weinheim (Germany): WILEY-VCH GmbH; 2024. p. 303–332
2. Wu X, Luo XC, Cheng HL, Yang RX, Chen XY. Recent progresses on ion beam irradiation induced structure and performance modulation of two-dimensional materials. *Nanoscale*. 2023;15(20):8925–8947.
3. Tao HC, Xu SR, Zhang JC, Su HK, Gao Y, Zhang YC, Zhou H, Hao Y. Improved crystal quality and enhanced optical performance of GaN enabled by ion implantation induced high-quality nucleation. *Opt Express*. 2023;31(13):20850–20860.
4. Skopinski L, Kretschmer S, Ernst P, Herder M, Madauss L, Breuer L, Krasheninnikov AV, Schleberger M. Velocity distributions of particles sputtered from supported two-dimensional MoS_2 during highly charged ion irradiation. *Phys Rev B*. 2023;107(7):Article 075418.
5. Iveković D, Luketić KT, Vázquez H, Leino A, Djurabekova F, Nordlund K, Madauss L, Liebsch Y, Schleberger M, Karlušić M. Suspended nanoporous graphene produced by swift heavy ion bombardment. *Mater Chem Phys*. 2024;313:Article 128729.
6. Unsuree N, Phanphak S, Prajongtat P, Bunpheng A, Jitapunkul K, Kongputhon P, Srinoi P, Iamprasertkun P, Hirunpinyopas W. A review: Ion transport of two-dimensional materials in novel technologies from macro to nanoscopic perspectives. *Energies*. 2021;14(18):Article 5819.
7. Zhang X, Chen A, Chen LT, Zhou Z. 2D materials bridging experiments and computations for electro/photocatalysis. *Adv Energy Mater*. 2022;12(4):Article 2003841.
8. Patra L, Pandey R. Mechanical properties of 2D materials: A review on molecular dynamics based nanoindentation simulations. *Mater Today Commun*. 2022;31, Article 103623.
9. Monk J, Yang Y, Mendelev MI, Asta M, Hoyt JJ, Sun DY. Determination of the crystal-melt interface kinetic coefficient from molecular dynamics simulations. *Model Simul Mater Sci*. 2010;18(1):Article 015004.

10. Kavousi S, Novak BR, Moldovan D, Asle Zaeem M. Quantitative prediction of rapid solidification by integrated atomistic and phase-field modeling. *Acta Mater*. 2021;211:Article 116885.
11. Frank JT, Unke OT, Müller KR, Chmiela S. A Euclidean transformer for fast and stable machine learned force fields. *Nat Commun*. 2024;15(1):Article 6539.
12. Bourdarie S, Xapsos M. The near-earth space radiation environment. *IEEE Trans Nucl Sci*. 2008;55(4):1810–1832.
13. Cochran DJ, Boutte AJ, Campola MJ, Carts MA, Casey MC, Chen DK, LaBel KA, Ladbury RL, Lauenstein JM, Marshall CJ, et al. Recent total ionizing dose and displacement damage compendium of candidate electronics for NASA space systems. In: *IEEE Workshop on Radiation Effects Data*. IEEE; 2011. p. 23–32.
14. Vogl T, Sripathy K, Sharma A, Reddy P, Sullivan J, Machacek JR, Zhang L, Karouta F, Buchler BC, Doherty MW, et al. Radiation tolerance of two-dimensional material-based devices for space applications. *Nat Commun*. 2019;10(1):Article 1202.
15. Wen S, Huang P. *Principles of tribology*. Hoboken (NJ): Wiley; 2017.
16. Holmberg K, Andersson P, Erdemir A. Global energy consumption due to friction in passenger cars. *Tribol Int*. 2012;47:221–234.
17. Kolesov EA. Choosing a substrate for the ion irradiation of two-dimensional materials. *Beilstein J Nanotechnol*. 2019;10:531–539.
18. Xiao Y, Zhou MY, Zeng MQ, Fu L. Atomic-scale structural modification of 2D materials. *Adv Sci*. 2019;6(5):Article 1801501.
19. Khossossi N, Singh D, Ainane A, Ahuja R. Recent progress of defect chemistry on 2D materials for advanced battery anodes. *Chem Asian J*. 2020;15(21):3390–3404.
20. Lin YC, Björkman T, Komsa HP, Teng PY, Yeh CH, Huang FS, Lin KH, Jadczak J, Huang YS, Chiu PW, et al. Three-fold rotational defects in two-dimensional transition metal dichalcogenides. *Nat Commun*. 2015;6(1):Article 6736.
21. Han SW, Yun WS, Kim H, Kim Y, Kim DH, Ahn CW, Ryu S. Hole doping effect of MoS_2 via electron capture of He^+ ion irradiation. *Sci Rep*. 2021;11(1):Article 23590.
22. Ochedowski O, Bukowska H, Soler VMF, Brökers L, Ban-d'Etat B, Lebius H, Schleberger M. Folding two dimensional crystals by swift heavy ion irradiation. *Nucl Instrum Methods Phys B*. 2014;340:39–43.
23. Pandey M, Ahuja R, Kumar R. Electron beam irradiation-induced atomically thin domes of two-dimensional materials: Graphene and MoS_2. *Surf Interfaces*. 2024;51:Article 104654.
24. Guo ZA, Zeng YH, Meng FX, Qu HZ, Zhang SL, Hu SP, Fan SD, Zeng HB, Cao R, Prasad PN, et al. In-situ neutron-transmutation for substitutional doping in 2D layered indium selenide based phototransistor. *eLight*. 2022;2(1):Article 9.
25. Tan Y, Liu XB, He ZL, Liu YR, Zhao MW, Zhang H, Chen F. Tuning of interlayer coupling in large-area graphene/WSe_2 van der Waals heterostructure via ion irradiation: Optical evidences and photonic applications. *ACS Photonics*. 2017;4(6):1531–1538.
26. Felix JF, da Silva AF, da Silva SW, Qu F, Qiu B, Ren JF, de Azevedo WM, Henini M, Huang CC. A comprehensive study on the effects of gamma radiation on the physical properties of a two-dimensional WS_2 monolayer semiconductor. *Nanoscale Horiz*. 2020;5(2):259–267.
27. Anbalagan AK, Hu FC, Chan WK, Gandhi AC, Gupta S, Chaudhary M, Chuang KW, Ramesh AK, Billo T, Sabbah A, et al. Gamma-ray irradiation induced ultrahigh room-temperature ferromagnetism in MoS_2 sputtered few-layered thin films. *ACS Nano*. 2023;17(7):6555–6564.
28. Kretschmer S, Maslov M, Ghaderzadeh S, Ghorbani-Asl M, Hlawacek G, Krasheninnikov AV. Supported two-dimensional materials under ion irradiation: The substrate governs defect production. *ACS Appl Mater Interfaces*. 2018;10(36):30827–30836.
29. Liu K, Hsin CL, Fu DY, Suh J, Tongay S, Chen M, Sun YH, Yan AM, Park J, Yu KM, et al. Self-passivation of defects: Effects of high-energy particle irradiation on the elastic modulus of multilayer graphene. *Adv Mater*. 2015;27(43):6841–6847.
30. Zaeem MA, Thomas S, Kavousi S, Zhang N, Mukhopadhyay T, Mahata A. Multiscale computational modeling techniques in study and design of 2D materials: Recent advances, challenges, and opportunities. *2D Mater*. 2024;11(4):Article 042004.
31. Kumar R, Mishra V, Dixit T, Sarangi SN, Samal D, Miryala M, Nayak PK, Rao MSR. Investigating the effect of H^+-ion irradiation on layered α-MoO_3 flakes by defect engineering. *Appl Phys Lett*. 2023;123(15):Article 151104.
32. Entani S, Larionov KV, Popov ZI, Takizawa M, Mizuguchi M, Watanabe H, Li ST, Naramoto H, Sorokin PB, Sakai S. Non-chemical fluorination of hexagonal boron nitride by high-energy ion irradiation. *Nanotechnology*. 2020;31(12): Article 125705.
33. Yao YF, Kononov A, Metzlaff A, Wucher A, Kalkhoff L, Breuer L, Schleberger M, Schleife A. Nonequilibrium dynamics of electron emission from cold and hot graphene under proton irradiation. *Nano Lett*. 2024;24(17):5174–5181.
34. Lin CP, Chen PC, Huang JH, Lin CT, Wang D, Lin WT, Cheng CC, Su CJ, Lan YW, Hou TH. Local modulation of electrical transport in 2D layered materials induced by electron beam irradiation. *ACS Appl Electron Mater*. 2019;1(5):684–691.
35. Weber WJ, Duffy DM, Thomé L, Zhang Y. The role of electronic energy loss in ion beam modification of materials. *Curr Opinion Solid State Mater Sci*. 2015;19(1):1–11.
36. Shi T. Ion irradiation effects on two-dimensional layered materials [thesis]. University of Michigan; 2019.
37. Ziegler JF, Ziegler MD, Biersack JP. SRIM—The stopping and range of ions in matter (2010). *Nucl Instrum Methods Phys Res, Sect B*. 2010;268(11–12):1818–1823.
38. Thomas LH. The calculation of atomic fields. *Proc Camb Phil Soc*. 1927;23(5):542–548.
39. Fermi E. A statistical method for determining some properties of the atoms and its application to the theory of the periodic table of elements. *Z Phys*. 1928;48(1–2):73–79.
40. Bohr N. *The penetration of atomic particles through matter*Munksgaard Copenhagen; 1948.
41. Jensen H. Die Ladungsverteilung in Ionen und die Gitterkonstante des Rubidiumbromids nach der statistischen Methode. *Z Phys*. 1932;77(11):722–745.
42. Moliere G. Theorie der streuung schneller geladener teilchen i. einzelstreuung am abgeschirmten coulomb-feld. *Zeitschrift für Naturforschung A*. 1947;2(3):133–145.
43. Ziegler JF, Biersack JP. The stopping and range of ions in matter. In: *Treatise on heavy-ion science. Volume 6: Astrophysics, chemistry, and condensed matter*. Springer; 1985. p. 93–129.

44. Sigmund P. Arriving at numbers. In: *Particle penetration and radiation effects: General aspects and stopping of swift point charges*. Germany: Springer; 2006. p. 229–273.
45. Firsov OB. A qualitative interpretation of the mean electron excitation energy in atomic collisions. *Sov Phys Jetp*. 1959;9(5):1076–1080.
46. Lindhard J, Scharff M. Energy dissipation by ions in Kev region. *Phys Rev*. 1961;124(1):128.
47. Brandt W, Kitagawa M. Effective stopping-power charges of swift ions in condensed matter. *Phys Rev B*. 1982;25(9): 5631–5637.
48. Schiwietz G, Grande PL. A unitary convolution approximation for the impact-parameter dependent electronic energy loss. *Nucl Instrum Meth B*. 1999;153(1–4):1–9.
49. Biersack JP. The effect of high charge states on the stopping and ranges of ions in solids. *Nucl Instrum Meth B*. 1993; 80–81(Part 1):12–15.
50. Schenkel T, Briere MA, Barnes AV, Hamza AV, Bethge K, SchmidtBocking H, Schneider DH. Charge state dependent energy loss of slow heavy ions in solids. *Phys Rev Lett*. 1997;79(11):2030–2033.
51. Wilhelm RA, Möller W. Charge-state-dependent energy loss of slow ions. II. Statistical atom model. *Phys Rev A*. 2016;93(5):Article 052709.
52. Stillinger FH, Weber TA. Computer-simulation of local order in condensed phases of silicon. *Phys Rev B*. 1985;31(8):5262–5271.
53. Tersoff J. New empirical-approach for the structure and energy of covalent systems. *Phys Rev B*. 1988;37(12):6991–7000.
54. Byggmästar J, Hamedani A, Nordlund K, Djurabekova F. Machine-learning interatomic potential for radiation damage and defects in tungsten. *Phys Rev B*. 2019;100(14): Article 144105.
55. Wang H, Guo X, Zhang LF, Wang H, Xue JM. Deep learning inter-atomic potential model for accurate irradiation damage simulations. *Appl Phys Lett*. 2019;114(24):Article 244101.
56. Roy A, Nandipati G, Casella AM, Senor DJ, Devanathan R, Soulami A. A review of displacement cascade simulations using molecular dynamics emphasizing interatomic potentials for TPBAR components. *NPJ Mat Degrad*. 2025;9(1):1.
57. Chu GS, Li Y, Zhao RC, Ren S, Yang W, He XF, Hu CJ, Wang J. MD simulation of hundred-billion-metal-atom cascade collision on Sunway Taihulight. *Comput Phys Commun*. 2021;269:108128.
58. Lehtinen O, Kotakoski J, Krasheninnikov AV, Keinonen J. Cutting and controlled modification of graphene with ion beams. *Nanotechnology*. 2011;22(17): https://doi.org/10.1088/0957-4484/22/17/175306
59. Wu X, Zhu XB. Molecular dynamics simulations of ion beam irradiation on graphene/MoS_2 heterostructure. *Sci Rep*. 2021;11(1):Article 21113.
60. Chen YR, Xia CJ, Song J, Sima RH, Zhou JJ, Liu Y, Tian XF, Zhang QX, Hao XP. Effect of cosmic rays irradiation on the phase change characteristics of an on-orbit fixed point. *Eur Phys J C*. 2023;83(1):Article 175306.
61. Aziz MA, Riyatun AF, Khakim A. Distribution dose absorption simulation of brachytherapy prostate using software Monte Carlo N' particle code extended (MCNPX) with seed implant model IsoAid Advantage™ IAI-125A. *AIP Conf Proc*. 2018;2011:Article 020034.
62. Caro A, Victoria M. Ion-electron interaction in molecular-dynamics cascades. *Phys Rev A*. 1989;40(5):2287–2291.
63. Finnis MW, Agnew P, Foreman AJE. Thermal excitation of electrons in energetic displacement cascades. *Phys Rev B*. 1991;44(2):567–574.
64. Flynn CP, Averback RS. Electron-phonon interactions in energetic displacement cascades. *Phys Rev B*. 1988;38(10):7118–7120.
65. Kaganov M. Relaxation between electrons and the crystalline lattice. *Sov Phys JETP*. 1957;4:173–178.
66. Darkins R, Duffy DM. Modelling radiation effects in solids with two-temperature molecular dynamics. *Comput Mater Sci*. 2018;147:145–153.
67. Shi T, Xu XQ, Wan H, Jia P, Zhang P, He H, Gao R, Lu CY. Modeling swift heavy ion irradiation of substrate-supported two-dimensional material via two-temperature molecular dynamics simulations. *AIP Adv*. 2024;14(8):Article 085322.
68. Mei ZG, Ponciroli R, Petersen A. Wigner energy in irradiated graphite: A first-principles study. *J Nucl Mater*. 2022;563.
69. Mo JL, Li L, Li XD, Feng QY, Xiang X, Deng HX, Nie JL, Zu XT. First-principles study on the microstructure, band structure, mechanical and optical properties of AB-stacked bilayer graphene under constant neutron irradiation with different electric field magnitudes and directions. *Mater Today Commun*. 2024;40:109932.
70. Möller W, Eckstein W, Biersack J. Tridyn-binary collision simulation of atomic collisions and dynamic composition changes in solids. *Comput Phys Commun*. 1988;51(3):355–368.
71. Nordlund K, Djurabekova F. Multiscale modelling of irradiation in nanostructures. *J Comput Electron*. 2014;13:122–141.
72. Åhlgren E, Kotakoski J, Lehtinen O, Krasheninnikov A. Ion irradiation tolerance of graphene as studied by atomistic simulations. *Appl Phys Lett*. 2012;100(23):233108.
73. Zhao S, Xue J. Tuning the band gap of bilayer graphene by ion implantation: Insight from computational studies. *Phys Rev B Condens Matter Mater Phys*. 2012;86(16):Article 165428.
74. Kretschmer S, Ghaderzadeh S, Facsko S, Krasheninnikov AV. Threshold ion energies for creating defects in 2D materials from first-principles calculations: Chemical interactions are important. *J Phys Chem Lett*. 2022;13(2):514–519.
75. Ma L, Tan Y, Ghorbani-Asl M, Boettger R, Kretschmer S, Zhou S, Huang Z, Krasheninnikov AV, Chen F. Tailoring the optical properties of atomically-thin WS_2via ion irradiation. *Nanoscale*. 2017;9(31):11027–11034.
76. Kretschmer S, Krasheninnikov A. Atomistic simulations of low energy ion irradiation of 2D materials: From molecular dynamics to simple binary collision model. *Phys Rev Mater*. 2024;8(11):Article 114003.
77. Fekri Z, Chava P, Hlawacek G, Ghorbani-Asl M, Kretschmer S, Awan W, Mootheri V, Venanzi T, Sycheva N, George A, et al. Tuning the electronic characteristics of monolayer MoS_2-based transistors by ion irradiation: The role of the substrate. *Adv Electron Mater*. 2024;10(9):025078.
78. Ghorbani-Asl M, Kretschmer S, Spearot DE, Krasheninnikov AV. Two-dimensional MoS_2 under ion irradiation: From controlled defect production to electronic structure engineering. *2D Mater*. 2017;4(2):Article 025078.
79. Jing NN, Xue QZ, Ling CC, Shan MX, Zhang T, Zhou XY, Jiao ZY. Effect of defects on young's modulus of graphene sheets: A molecular dynamics simulation. *RSC Adv*. 2012;2(24):9124–9129.
80. Li TZ, Zhi GX, Chen C, Zhang L, Zhai SW, Dou WZ, Wu JE, Hu WJ, Zhou M. Ion irradiation effects on two-dimensional

MXene Ti_2C for applications in extreme conditions: Combined ab initio and Monte Carlo simulations. *ACS Appl Nano Mater*. 2023;6(5):3463–3471.
81. Li TZ, Gao WJ, Zhi GX, Zhai SW, Xu JH, Zhang L, Hu WJ, Song BY, Xu SK, Zhou M. I2DM: A Monte Carlo framework for ion irradiation on two-dimensional materials. *Comput Phys Commun*. 2025;308:109445.
82. Ojanperä A, Krasheninnikov AV, Puska M. Electronic stopping power from first-principles calculations with account for core electron excitations and projectile ionization. *Phys Rev B*. 2014;89(3):035120.
83. Bubin S, Wang B, Pantelides S, Varga K. Simulation of high-energy ion collisions with graphene fragments. *Phys Rev B*. 2012;85(23):Article 235435.
84. Kretschmer S, Krasheninnikov A. Electron irradiation of two-dimensional MoS_2: Insights into the influence of electronic excitations from first-principle calculations. *Microsc Microanal*. 2020;26(S2):784–785.
85. Mortensen JJ, Larsen AH, Kuisma M, Ivanov AV, Taghizadeh A, Peterson A, Haldar A, Dohn AO, Schäfer C, Jonsson EÖ, et al. GPAW: An open python package for electronic structure calculations. *J Chem Phys*. 2024;160(9):Article 092503.
86. Batignani G, Bettarini S, Borghi G, Boscardin M, Ciarrocchi A, Crivellari M, Coletti C, Di Gaspare A, Di Lieto A, Forti F. Development of graphene-based ionizing radiation sensors. *Nucl Instrum Methods Phys Res Sect A*. 2019;936:666–668.
87. Jain S, Gajarushi AS, Gupta A, Rao VR. A passive gamma radiation dosimeter using graphene field effect transistor. *IEEE Sensors J*. 2019;20(6):2938–2944.
88. Stará V, Procházka P, Mareček D, Šikola T, Čechal J. Ambipolar remote graphene doping by low-energy electron beam irradiation. *Nanoscale*. 2018;10(37):17520–17524.
89. Zhang EX, Newaz A, Wang B, Bhandaru S, Zhang CX, Fleetwood DM, Bolotin KI, Pantelides ST, Alles ML, Schrimpf RD. Low-energy X-ray and ozone-exposure induced defect formation in graphene materials and devices. *IEEE T Nucl Sci*. 2011;58(6):2961–2967.
90. Zhang E, Newaz A, Wang B, Zhang C, Fleetwood D, Bolotin K, Schrimpf R, Pantelides S, Alles M. Ozone-exposure and annealing effects on graphene-on-SiO_2 transistors. *Appl Phys Lett*. 2012;101(12):Article 121601.
91. Puzyrev Y, Wang B, Zhang E, Zhang C, Newaz A, Bolotin K, Fleetwood D, Schrimpf R, Pantelides S. Surface reactions and defect formation in irradiated graphene devices. *IEEE Trans Nucl Sci*. 2012;59(6):3039–3044.
92. Francis SA, Petrosky JC, McClory JW, Cress CD. Effects of proton and X-ray irradiation on graphene field-effect transistors with thin gate dielectrics. *IEEE Trans Nucl Sci*. 2014;61(6):3010–3017.
93. Zhang CX, Wang B, Duan GX, Zhang EX, Fleetwood DM, Alles ML, Schrimpf RD, Rooney AP, Khestanova E, Auton G. Total ionizing dose effects on hBN encapsulated graphene devices. *IEEE Trans Nucl Sci*. 2014;61(6):2868–2873.
94. Zeng J, Ma P, Zhang S, Xu L, Li Z, Zhai P, Hu P, Maaz K, Sun Y, Liu J. Unrecovered ion-irradiated damage after thermal annealing in graphene field effect transistors. *Appl Surf Sci*. 2022;588:Article 153005.
95. Iqbal M, Hussain G, Kamran M, Aslam I, Alharbi T, Azam S, Majid A, Razzaq S. Effect of E-beam irradiation on graphene sandwiched between h-BN layers. *Microelectron Eng*. 2019;216:Article 111044.
96. Zhang Y, Peng S, Wang Y, Guo L, Zhang X, Huang H, Su S, Wang X, Xue J. Environment-dependent radiation tolerance of graphene transistors under proton irradiation. *J Phys Chem Lett*. 2022;13(46):10722–10727.
97. Wang ZH, Zhou XZ, Sun BX, Zhang WG, Su XJ, Shi JK, Huang QH. Model construction and dominant mechanism analysis of Li-ion batteries under periodic excitation. *Space Sci Tech China*. 2024;4:Article 0129.
98. Mak KF, Lee C, Hone J, Shan J, Heinz TF. Atomically thin MoS_2: A new direct-gap semiconductor. *Phys Rev Lett*. 2010;105(13):Article 136805.
99. Kuc A, Zibouche N, Heine T. Influence of quantum confinement on the electronic structure of the transition metal sulfide TS_2. *Phys Rev B Condens Matter Mater Phys*. 2011;83(24):Article 245213.
100. Kang Y, Jeon D, Kim T. Local mapping of the thickness-dependent dielectric constant of MoS_2. *J Phys Chem C*. 2021;125(6):3611–3615.
101. Donetti L, Marquez C, Navarro C, Medina-Bailon C, Padilla JL, Sampedro C, Gamiz F. Towards a DFT-based layered model for TCAD simulations of MoS_2. *Solid State Electron*. 2022;197:Article 108437.
102. Mirabelli G, Hurley PK, Duffy R. Physics-based modelling of MoS_2: The layered structure concept. *Semicond Sci Technol*. 2019;34(5):Article 055015.
103. Wang P, Perini C, O'Hara A, Tuttle B, Zhang E, Gong H, Liang C, Jiang R, Liao W, Fleetwood D. Radiation-induced charge trapping and low-frequency noise of graphene transistors. *IEEE Trans Nucl Sci*. 2017;65(1):156–163.
104. Cress CD, Champlain JG, Esqueda IS, Robinson JT, Friedman AL, McMorrow JJ. Total ionizing dose induced charge carrier scattering in graphene devices. *IEEE T Nucl Sci*. 2012;59(6):3045–3053.
105. Li JF, Guo HX, Ma WY, Song HJ, Zhong XL, Li YF, Bai RX, Lu XJ, Zhang FQ. Total x-ray dose effect on graphene field effect transistor. *Acta Phys Sin*. 2024;73(5):Article 058501.
106. Boahen JK, Mohamed SAE, Khalil ASG, Hassan MA. Application of artificial intelligence techniques in modeling attenuation behavior of ionization radiation: A review. *Radiat Detect Techno*. 2023;7(1):56–83.
107. Jinia AJ, Clarke SD, Moran JM, Pozzi SA. Intelligent radiation: A review of machine learning applications in nuclear and radiological sciences. *Ann Nucl Energy*. 2024;201.
108. Fu ZC, Sun BX, Gong J, Gong MM, Zhao XZ, Ma SC. A SOC estimation method for Li-ion batteries under high-rate pulse conditions based on AO-BPNN model. *Space-Sci Tech-China*. 2023;3:0088.
109. Mishin Y. Machine-learning interatomic potentials for materials science. *Acta Mater*. 2021;214:Article 116980.
110. Xu BH, Hua GB, Qian C, Xia Q, Sun B, Ren Y, Wang ZL. Determining maximum allowable current of an RBS using a directed graph model and greedy algorithm. *Space-Sci Tech-China*. 2024;4:Article 0122.
111. Guo RQ, Li GT, Tang JL, Wang YL, Song XH. Small-data-based machine learning interatomic potentials for graphene grain boundaries enabled by structural unit model. *Carbon Trends*. 2023;11:Article 100260.
112. Pun GPP, Yamakov V, Hickman J, Glaessgen EH, Mishin Y. Development of a general-purpose machine-learning interatomic potential for aluminum by the physically informed neural network method. *Phys Rev Mater*. 2020;4(11):Article 113807.

113. Lin YS, Pun GPP, Mishin Y. Development of a physically-informed neural network interatomic potential for tantalum. *Comput Mater Sci*. 2022;205:Article 111180.
114. Zheng BW, Gu GX. Machine learning-based detection of graphene defects with atomic precision. *Nano Micro Lett*. 2020;12(1):Article 181.
115. Jinnouchi R, Karsai F, Kresse G. On-the-fly machine learning force field generation: Application to melting points. *Phys Rev B*. 2019;100(1):Article 014105.
116. Dash AK, Swaminathan H, Berger E, Mondal M, Lehenkari T, Prasad PR, Watanabe K, Taniguchi T, Komsa HP, Singh A. Evidence of defect formation in monolayer MoS_2 at ultralow accelerating voltage electron irradiation. *2D Mater*. 2023;10(3): https://doi.org/10.1103/physrevb.100.014105
117. Wines D, Choudhary K. CHIPS-FF: Evaluating universal machine learning force fields for material properties. *ACS Mater Lett*. 2025;7(6):2105–2114.
118. Lu B, Xia YZ, Ren YQ, Xie MM, Zhou LG, Vinai G, Morton SA, Wee ATS, van der Wiel WG, Zhang W, et al. When machine learning meets 2D materials: A review. *Adv Sci*. 2024;11(13):Article 2305277.
119. Stassinopoulos EG, Raymond JP. The space radiation environment for electronics. *P IEEE*. 1988;76(11):1423–1442.

Space: Science & Technology
A SCIENCE PARTNER JOURNAL

Multiscale Modeling Techniques in the Study of 2-Dimensional Materials under Ionizing Radiation

Hongyu Tang, Zihao Cai, Mengyuan Tang, Ninghai Yu, Weiqi Shi, Lindong Ma, Jiajie Fan, Rongjun Zhang, and Guoqi Zhang

Citation: Tang H, Cai Z, Tang M, Yu N, Shi W, Ma L, Fan J, Zhang R, Zhang G. Multiscale Modeling Techniques in the Study of 2-Dimensional Materials under Ionizing Radiation. *Space Sci Technol*. 2026;**6**:0403. DOI: 10.34133/space.0403

Two-dimensional materials (2DMs)-based devices exhibit aerospace potential due to their superior properties. However, the operational reliability of 2DMs-based devices in space environments is significantly influenced by charged-particle radiation, necessitating rigorous ground-based radiation tolerance assessments. Current research on radiation effects in 2DMs is primarily experimental, yet such methodologies are inherently time-consuming, resource-intensive, and limited in throughput. To address these challenges, computational modeling and simulation techniques are increasingly being integrated with experimental characterization to accelerate materials design and unravel underlying physical mechanisms. This review systematically evaluates the state-of-the-art multiscale computational frameworks for 2DMs research, focusing on recent advancements, technical challenges, and emerging opportunities. A novel integrative approach is proposed, combining density functional theory, molecular dynamics, Monte Carlo, finite element analysis, and machine learning techniques. Particular emphasis is placed on addressing challenges in multiscale modeling, including accurate representation of complex phenomena across spatial and temporal scales under extreme environmental conditions. Conversely, opportunities for enhancing predictive capabilities are highlighted, with implications for expediting materials discovery in electronics, photonics, energy storage, catalysis, and nanomechanical systems. This comprehensive survey provides a strategic roadmap for future research directions in multiscale computational modeling of 2DMs, emphasizing interdisciplinary methodologies that bridge atomistic simulations with macroscale engineering applications. The insights presented herein aim to advance the development of radiation-hardened 2DMs-based devices for next-generation aerospace systems.
Image

Space: Science & Technology (ISSN 2692-7659) is published by the American Association for the Advancement of Science. 1200 New York Avenue NW, Washington, DC 20005.